



British Geological Survey

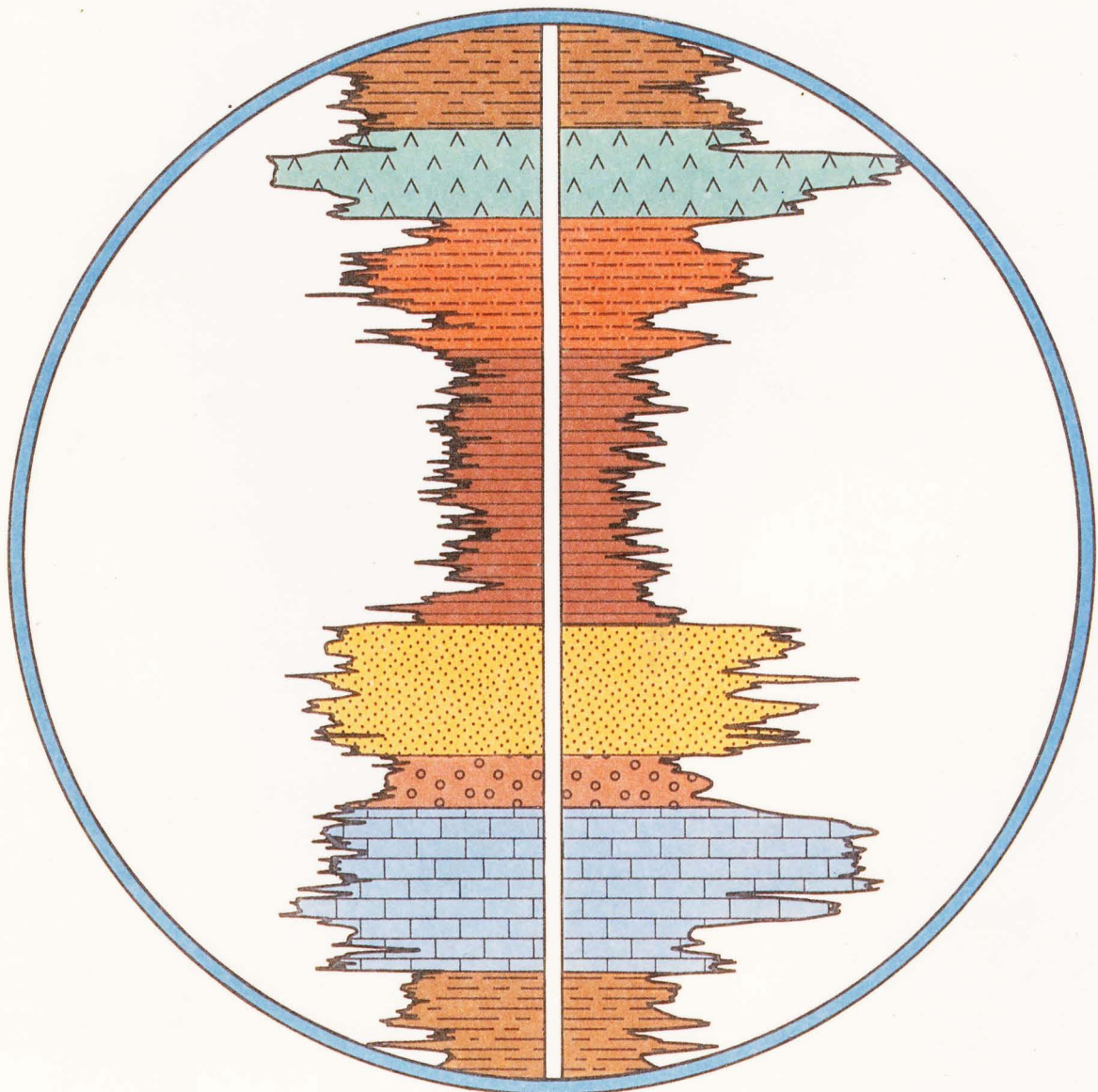
REGIONAL GEOPHYSICS RESEARCH GROUP

Technical Report WK/90/11

Regional Geophysics Series

# Physical properties of sediments and basalts from the Argo and Gascoyne Abyssal Plains in the Indian Ocean

N R Brereton



This report has been generated from a scanned image of the document with any blank pages removed at the scanning stage.  
Please be aware that the pagination and scales of diagrams or maps in the resulting report may not appear as in the original

British Geological Survey  
Natural Environment Research Council

Technical Report WK/90/11

Regional Geophysics Series

**Physical properties of sediments and  
basalts from the Argo and Gascoyne  
Abyssal Plains in the Indian Ocean**

N R Brereton

Regional Geophysics Research Group

*Bibliographic reference*

BRERETON, N R. 1990. Physical properties of sediments and basalts from the Argo and Gascoyne Abyssal Plains in the Indian Ocean. *British Geological Survey Technical Report WK/90/11*.

## SUMMARY

The Wyllie time average equation has, for many years, been universally applied to predict porosities from compressional wave velocities, or visa-versa. However, it has long been recognized that the Wyllie equation does not adequately describe the actual relationship between these two parameters, and there have been many attempts to improve upon it. These have included the use of a simplified Wood equation, the concept of acoustic formation factor, and a wide range of empirical relationships. In many cases these models have been derived by testing them against a set of data representing a relatively narrow range of porosity values and, similarly, the use of the Wyllie equation has often been justified by virtue of a pseudo-linear relationship over a narrow range of porosity values.

During the Ocean Drilling Program - Leg 123 two sites were drilled in the deep Indian Ocean. Continuous coring at Site 765 recovered over 930m succession of soft Quaternary through Lower Cretaceous sediments and a further 271m of oceanic basement with relatively fresh, glass-bearing pillow lava and massive basalt. Soon after core recovery, measurements were made of: saturated bulk density, grain density, water content, porosity, and compressional wave velocity. The porosity ranged from 89%, close to the sea floor, to 1.6% for the dense basalts. This self consistent set of measurements made on fresh samples, with a wide range of values, has enabled some of the descriptive models to be tested more rigorously.

Some of the limitations of the time average equation were also recognised by Wyllie and his co-workers who amended the Wood emulsion equation to partially take account of the rigidity of the materials. Further modifications to this Wyllie-Wood equation have been shown here to not only describe the relationship between porosity and velocity more closely than the time average equation, but also more closely than some of the alternative proposals suggested by contemporaries of Wyllie and since. Indeed, bearing in mind the Wyllie-Wood equation was discussed in the same paper the time average equation was first proposed, it is somewhat curious that the time average equation has been adhered to for so long.

A semi-empirical acoustic impedance relationship has been developed which is shown to provide a more accurate porosity-velocity transform than has hitherto been possible using realistic material parameters.

## CONTENTS

- 1 INTRODUCTION
- 2 PHYSICAL PROPERTY MEASUREMENTS
- 3 GEOLOGICAL SUMMARIES
  - 3.1 Site 765
    - 3.1.1 Sediments
    - 3.1.2 Basalts
  - 3.2 Site 766
    - 3.2.1 Sediments
    - 3.2.2 Basalts
- 4 INDEX PROPERTIES
  - 4.1 General Relationships
  - 4.2 ODP Leg 123 Data
    - 4.2.1 Data Discrepancies
    - 4.2.2 Corrections to the Data
  - 4.3 Index Property Correlations
- 5 POROSITY - VELOCITY TRANSFORMS
  - 5.1 Background
  - 5.2 The Acoustic Impedance Transform
- 6 THERMAL CONDUCTIVITY RELATIONSHIPS
- 7 DISCUSSION AND CONCLUSIONS
- 8 ACKNOWLEDGEMENTS
- 9 REFERENCES

## 1 INTRODUCTION

Between August 31 and November 1 1988 Leg 123 of the Ocean Drilling Program (ODP) investigated two sites in the deep Indian Ocean northwest of the Australian continental margin. The first of these (Site 765), is at the southern limit of the Argo Abyssal Plain within 50 Km of the Exmouth Plateau and the second (Site 766), about 850 Km to the southwest (Fig. 1), is at the boundary between the ocean crust of the Cuvier and Gascoyne abyssal plains and the continental crust of the Exmouth Plateau.

One of the primary objectives of ODP Leg 123 was to drill the oldest sediments and basement of the Indian Ocean in the Argo Abyssal Plain to understand the paleoceanography, sedimentology, and magmatic processes relating to rifting of the northwestern Australian margin, the initiation of the Indian Ocean and the consequent destruction of the Tethyan seas. An important secondary objective was to create a geochemical reference site for ocean crust composition close to a subduction zone.

At Site 765 calcareous turbidites constituted more than 75% of the section, alternating with hemipelagic claystones, but the most surprising stratigraphic finding was the lack of any Jurassic sediments. Initial results indicate that the Indian Ocean opening started about 20 Ma later than had previously been thought (Berriasian-Valanginian as opposed to Oxfordian), requiring a significant revision of the plate-tectonic reconstruction of the northeastern Indian Ocean. The hole is in 5714 m of water and penetrated over 930 m of Cretaceous through Cenozoic sediments and a further 271 m of oceanic basement with relatively fresh, glass-bearing pillow lava and massive basalt. It was necessary to case-out the sediments before drilling the basement and this involved installing a re-entry cone. The drillship "JOIDES Resolution" achieved the deepest steel cased-hole in the worlds oceans and the hole has been left in excellent condition for further drilling on future legs.

Site 766, in 4 Km of water penetrated 220 m of locally derived terrigenous clastic fan deposits overlain by 240 m of pelagic ooze, chalk and chert. The basal sediments are intruded by basalt sills and a massive dyke, almost continuously recovered for about 60 m.

Preliminary results from the wide ranging scientific investigations carried out during the Leg 123 cruise are in preparation or have been briefly reported (ODP Leg 123 shipboard scientific party. 1989a, 1989b and 1990) but the principal findings are to be published in the Proceedings of the Ocean Drilling Program - Scientific Results (Vol 123).

## 2 PHYSICAL PROPERTY MEASUREMENTS

Physical properties determined on board ship were: porosity, bulk density, grain density and water content (collectively referred to as index properties); compressional wave velocity; and thermal conductivity. In addition, the Gamma Ray Attenuation Porosity Evaluator (GRAPE), described by Boyce (1976), was used to make a continuous measurement of wet-bulk density in cores taken with the hydraulic piston corer but these, together with measurements of the undrained shear strength and other properties will not be discussed further in this report.

Drilling technology employed by the ODP enables continuous coring of the softest sediments at the seawater-sediment boundary, right through to the hardest basalts. The cores were recovered in 10 m plastic sleeved core barrels thereby retaining the integrity of the softer materials.

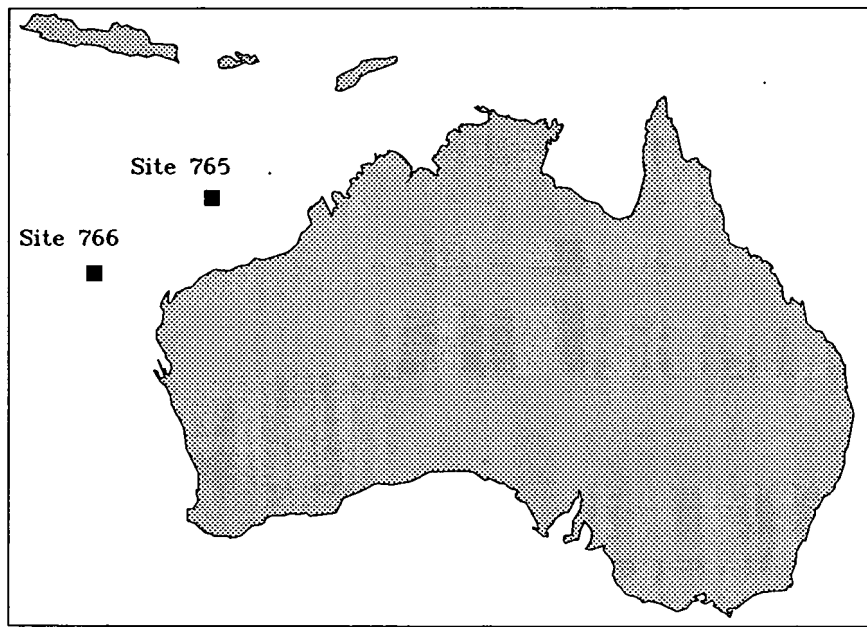


Figure 1 ODP Leg 123 Drilling Site Locations

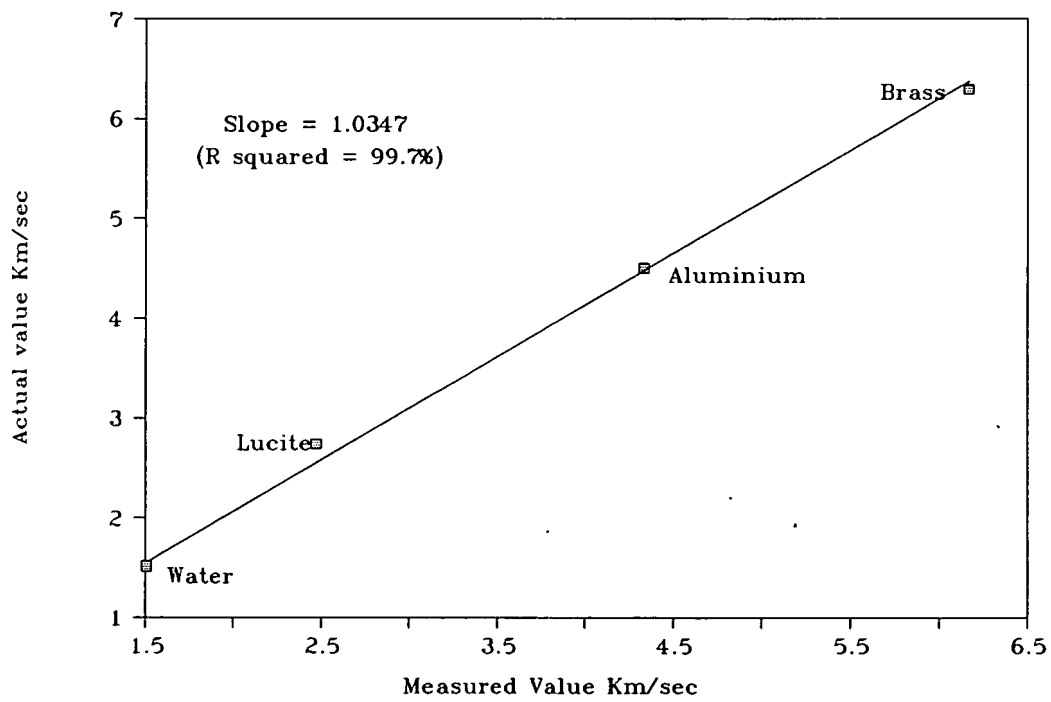


Figure 2 Compressional Wave Velocity – equipment calibration

Soon after core recovery, the plastic liners were cut into 1.5 m sections and each section split lengthwise. One half was archived while the other was used for sampling. Samples for index property and compressional wave velocity measurements were taken by either cutting parallel sided pieces with a knife in the softer sediments, or using a double bladed diamond saw for the more brittle or lithified sediments. Basement rock samples were obtained using a 2.5 cm rock corer. In almost all cases these two sets of measurements were made on the same samples. It was not practicable however, to also make thermal conductivity measurements on these same samples. At no time were the cores allowed to dry out prior to measurements being taken and sample temperatures were allowed to equilibrate with the stabilised laboratory temperature.

For the index property determinations samples were weighed wet using two Scientech 202 electronic balances, interfaced with a micro computer, which compensates for the ship's motion by taking the average of 100 sample weighings. The wet sample volumes were determined using a Quantachrome helium Penta-Pycnometer. Dry sample weights and volumes were determined using the same procedure after freeze drying the sample for 12 hours. The accuracy of the weight and volume determinations were periodically checked using calibration standards.

Compressional wave velocities were calculated from the determination of the travel time of a 500 kHz compressional wave through a measured thickness of sample using a Hamilton Frame Velocimeter and Tektronix DC 5010 counter/timer system. Travel distance was measured using an attached variable resistor connected to a Tektronix DM 5010 digital multimeter. The Hamilton Frame was calibrated with lucite, aluminium, brass, and water standards at the beginning of Leg 123 (Fig. 2). The variable resistor was calibrated with standard lengths of aluminium cylinders. It was found that a correction factor of 1.0347 was needed to bring all the measured values into agreement with the calibration values. Sea water velocity determined on this basis was about 1560 m/s.

The index property and compressional wave velocity data were entered into the shipboard Physical Properties Data Collection System which computes the depth below sea floor (mbsf), index properties and velocity for each sample.

The thermal conductivity techniques used have been described by Von Herzen and Maxwell (1959) and Vacquier (1985). Needle probes connected to a Thermcon-85 unit, interfaced with a micro-computer, were inserted into the sediment through holes drilled into the liner (before being split), and the thermal drift was monitored. An additional probe was inserted into a reference material. Once the temperature had stabilized, the probes were heated, and the coefficient of thermal conductivity was calculated as a function of the change in resistance in the probe. When the sediment became sufficiently lithified or when basement rock was tested, thermal conductivity was measured on samples taken from split cores placed on a slab of insulating material within which a needle probe was partially embedded.

### 3 GEOLOGICAL SUMMARIES

#### 3.1 Site 765

##### 3.1.1 Sediments

The sediments at Site 765 can be identified in terms of four basic physical properties units, namely, A (0-80 mbsf), B (80-350 mbsf), C (350-590 mbsf), and D (590-896 mbsf). No samples were taken from the

intervals 646-675 mbsf and 896-936 mbsf as these represented sensitive stratigraphic boundaries.

Unit A consists of calcareous ooze with significant changes in the index properties. The grain density remains relatively constant with an average value of  $2.62 \pm 0.13$  g/cm<sup>3</sup>. A distinct decrease in water content and porosity was observed from the mudline to 80 mbsf with a corresponding increase in bulk densities.

Unit B consists of debris flows and turbidites. Although the variability in porosity was considerably less, similar normal compaction trends with depth were observed. The grain densities increase slightly to  $2.71 \pm 0.11$  g/cm<sup>3</sup>. In the interval from 265-290 mbsf the general lithology consists of homogeneous clay deposits sandwiched between thinner layers of carbonate cemented sands.

Unit C consists of debris flows and turbidites with the sediments showing a much higher degree of lithification. The material alternates between claystone, chalk, and cemented sandstone with periodic intrusions of coarse sands and basalt pebbles. The index properties appeared to remain relatively constant throughout the unit, but showed a high degree of variability. The grain densities have an average value of  $2.70 \pm 0.13$  g/cm<sup>3</sup> and the water content decreases from roughly 35% at the top to 20% at the bottom of the unit. This variability can be attributed to measurements made in the layered calcareous claystone and cemented sandstones. In addition, a few measurements (at 465.56, 635.33 and 763.34 mbsf) were made on the basalt pebbles.

Unit D consists predominantly of a dark red claystone. The claystone is not as competent as the claystones in unit C and tended to slake or delaminate when exposed to water or became air dried. During sampling, the material had a "spongy" appearance. The boundary was readily distinguishable in terms of physical property changes. The profile as a whole showed the normal compaction trends, i.e., decreasing water content and porosity with a resulting increase in bulk density as function of increasing depth. The average grain density for the interval is  $2.66 \pm 0.14$  g/cm<sup>3</sup>.

The compressional wave velocity data showed an underlying trend of progressively increasing velocities, from approximately 1525 m/s in the calcareous ooze near the sea bottom sediment boundary, to about 2010 m/s near the sediment-basement boundary. Superimposed on this trend are a series of high and low velocity excursions. The higher values are associated with lithified claystone, chalk or cemented sandstone, whereas low values are indicative of less lithified claystone, carbonates or poorly cemented sandstone. The variability in the data is also, in part, a result of the sampling procedure followed. Samples were taken to be as representative as possible of the sediment section as a whole. In the case of a turbidite or debris flow sequence, both the upper fine grained and lower coarse grained sequences were selected. Sample selection also depended upon the relative frequency, thickness, and homogeneity of a particular sequence; thin, unrepresentative lithologies were avoided. Basalt pebbles occurred relatively frequently in the debris flow sequences, and were sampled at 465.56, 635.33 and 763.34 mbsf. These data represent significant spikes in the trends.

A series of high velocity peaks were observed between 350-450 mbsf. These peaks appear to be superimposed on a slight velocity increase between 350-590 mbsf and closely correspond to intermediate depth high amplitude reflectors recorded on the seismic survey lines (ODP Leg 123 Initial Reports volume). In addition, this section corresponds to the increased lithification of the sediments composing the turbidite and debris flow sequences. There is also a sharp decrease in velocity between 585.19 and 593.04 mbsf which also corresponds to a low amplitude

reflector on the seismic profile. The index properties for this interval show a significant variation, namely, an increase in porosity and water content and decrease in bulk density.

### 3.1.2 Basalts

The basement rocks were relatively homogeneous and composed primarily of pillow basalts and massive basalt flows. The water content and porosity data show significant variability but also remain relatively constant with depth. A sharp increase in water content and porosity occurred at 994 and 1005 mbsf with corresponding reductions in the measured velocity. These samples appeared lighter in colour and had a much coarser grain structure when compared with the other basalts. A reduction in velocity for the sample from 1140 mbsf corresponds to an interval in which a number of calcite veins were observed. A large variation in the index properties occurred at 1162 mbsf. The sample does not appear to be different from the surrounding material, namely, dark fine grained basalt; therefore, these data are believed to be suspect.

## 3.2 Site 766

### 3.2.1 Sediments

The sediments at Site 766 can be identified in terms of five basic physical properties units, namely, A (0-100 mbsf), B (100-185 mbsf), C (185-240 mbsf), D (240-300 mbsf), and E (300-459 mbsf).

Unit A consists of calcareous ooze with significant changes in the index properties in the upper 22 mbsf, followed by more gradual changes which are consistent with normal compaction trends. The grain density remains relatively constant with an average value of  $2.66 \pm 0.10$  g/cm<sup>3</sup> while distinct decreases in water content and porosity were observed.

Unit B consists of mixed sediment of claystone and chalk for which there was a greater variability in index properties. The average grain density increases to  $2.78 \pm 0.14$  g/cm<sup>3</sup>.

Unit C consists predominantly of chalk with hard chert layers. The grain densities decrease, having an average value of  $2.47 \pm 0.19$  g/cm<sup>3</sup>, while the porosities and water contents showed considerable variation, depending upon the type of material encountered.

Unit D consists predominantly of a dark brown to reddish brown claystone which tended to slake or delaminate when exposed to water or became air dried. In general, the grain densities increase with depth from roughly  $2.5$  g/cm<sup>3</sup> in the carbonate rich material, to near  $2.7$  g/cm<sup>3</sup> at the lower boundary. Both water content and porosity appeared to be slightly higher than the surrounding units.

Unit E is composed primarily of green to gray glauconitic siltstones and sandstones with periodic layers of highly lithified bioclastic sandstone. Although the index properties basically remained constant with depth, they were highly variable due to the layered nature of the material. The average grain density is  $2.71 \pm 0.08$  g/cm<sup>3</sup>. The lowermost 20 m consists of a gray to black clayey sandstone, although the index properties for this layer did not vary significantly from those described for the unit as a whole.

The compressional wave velocity progressively increases to about 1900 m/s near the sediment-basement boundary. Superimposed on this trend were a series of high velocity excursions associated with the layers of chert and lithified bioclastic sandstone. The low velocity sample from 141 mbsf also corresponded to marked changes in the index properties and came from a less well lithified chalk section of a mixed

sediment claystone-chalk sequence. Two velocity spikes at 201 and 222 mbsf corresponded to chert. At 300 mbsf and in the interval from 350 to 440 mbsf another series of velocity peaks correlated with highly lithified bioclastic sandstone layers.

### 3.2.2 Basalts

The igneous rocks drilled at Site 766 consist of three basic units, namely, A (460-463 mbsf), B (463-467 mbsf), and C (467-516 mbsf).

Unit A is a thin basalt sill. The index properties varied considerably from the outside edges toward the centre. The grain densities at the upper and lower boundaries have an average value of 2.68 g/cm<sup>3</sup>, whereas the value in the centre of the sill is 2.84 g/cm<sup>3</sup>. The water content and porosity also decreased from the outer boundaries towards the centre.

Unit B comprises a thin dark shale sediment layer, which was very similar to that observed in the lowermost portion of the sediment column.

Unit C consists of a thick diabase sill. Although there is some variation in the index properties in the uppermost portion, the values for the majority of the unit remained relatively constant with little variation. The average grain density is 2.91 ± 0.05 g/cm<sup>3</sup>.

Velocities for the uppermost basalt unit vary considerably from about 4200 m/s, at the upper and lower boundaries, to 5179 m/s at the centre. Within the sediment layer the velocity decreases significantly to an average value of 1848 m/s while the lowermost basalt unit shows some slight variations in the velocities, with an average of 5450 m/s.

## 4 INDEX PROPERTIES

### 4.1 General Relationships

During the course of analysing the data collected during Leg 123, it became clear that there were inconsistencies. These will be discussed in the next section but in order to understand the inconsistencies it is necessary to understand the derivation of the general relationships between the index properties.

The index properties are determined from four measurements; wet volume  $V_w$ , dry volume  $V_d$ , wet weight  $M_w$ , and dry weight  $M_d$ . These are defined as:

$$V_w = V_f + V_h + V_g \quad (a)$$

$$V_d = V_h + V_g \quad (b)$$

$$M_w = M_f + M_h + M_g \quad (c)$$

$$M_d = M_h + M_g \quad (d)$$

where subscripts f, h, and g refer to the fluid or pore water content, the salt in solution in the fluid, and the matrix or grain values. The relationships used in the shipboard Physical Properties Data Collection

System to calculate the index properties were corrected for salt content by assuming a pore water salinity of 36.3 ppt and a pore water density of 1.0245 g/cm<sup>3</sup>. Therefore:

$$M_h = 0.0363 M_f \quad (e)$$

$$\rho_p = \frac{(M_f + M_h)}{V_p} = 1.0245 \quad (f)$$

and

$$\rho_h = \frac{M_h}{V_h} = 2.25 \quad (g)$$

where

$$V_p = V_f + V_h \quad (h)$$

and  $\rho_p$  is the pore fluid density,  $\rho_h$  is the salt density and  $V_p$  is the pore fluid volume.

The definitions used for the index properties are:

Porosity = volume of water / volume of wet core;

Bulk Density = weight of wet core / volume of wet core;

Grain Density = weight of dry core / volume of dry core;

Water Content = weight of water / dry weight of core;

From these definitions the following relationships can be derived:

Porosity

$$\phi = \frac{V_p}{V_w} = \frac{1.0363(M_w - M_d)}{V_w \rho_f} \quad (1)$$

Bulk Density (saturated)

$$\rho_s = \frac{M_w}{V_w} \quad (2)$$

Grain Density

$$\rho_g = \frac{M_g}{V_g} = \frac{M_d - 0.0363(M_w - M_d)}{V_d - 0.0161(M_w - M_d)} \quad (3)$$

Water Content

$$W = \frac{(M_f + M_h)}{M_g} = \frac{1.0363(M_w - M_d)}{M_w - 1.0363(M_w - M_d)} \quad (4)$$

From equations 1, 2, 3 and f it can be shown that:

$$\rho_s = \rho_p \phi + \rho_g (1 - \phi) \quad (5)$$

which can be written in a more convenient form as;

$$\rho_s = \phi(\rho_p - \rho_g) + \rho_g \quad (6)$$

From equations 1, 4, and f it can be shown that:

$$W = \frac{\rho_p \phi}{\rho_g (1 - \phi)} \quad (7)$$

and from 5:

$$\rho_s = \rho_p \phi \frac{(W + 1)}{W} \quad (8)$$

and also from 7:

$$\rho_s = \rho_g (1 - \phi)(W + 1) \quad (9)$$

## 4.2 ODP Leg 123 Data

### 4.2.1 Data Discrepancies

Index properties were determined from measurements carried out during the course of Leg 123. A preliminary qualitative assessment of the results was discussed in Proceedings of the Ocean Drilling Program - Initial Reports Volume 123 (1990), and an indication of the general stratigraphical zoning was described. All the index properties determined during the cruise were tabulated.

When reducing the index properties data for the basalts and basement rocks it was found that in a significant number of instances the dry volume exceed the wet volume. Since this results in the grain density being less than the bulk density, it clearly cannot be so. At the time, this discrepancy between the wet and dry volumes was attributed to the very low porosities of the basalts resulting in their difference being less than the accuracy of the pycnometer. Therefore in calculating the index properties, the wet or total volume was determined using an averaged sample diameter and height, as measured to the nearest 0.002 cm by a set of calipers. This volume, along with the wet and dry weights, was used to calculate the index properties for the basalts and basement rocks. These are the results that are presented in Initial Reports Volume 123 (1990).

Equation 6 above is a linear relationship which, for a plot of  $\rho_s$  against  $\phi$ , should yield an intercept of  $\rho_g$  and a slope of  $(\rho_p - \rho_g)$ . Such a plot for all the sediments data from Sites 765 and 766 gives an intercept (ie grain density) of 2.899 g/cm<sup>3</sup> and a derived value of pore fluid density of 1.176 g/cm<sup>3</sup>. However, the average value of the measured grain density is 2.677 g/cm<sup>3</sup>, which is very close to the expected value, and all the index properties are determined on the basis of an assumed value of pore fluid density of 1.0245 g/cm<sup>3</sup>. Therefore, there is a discrepancy in the use of equation 6.

Similarly, from equation 8 a plot of  $\rho_s$  against  $\phi(W+1)/W$  should yield a value for the slope similar to the pore fluid density of about 1.0245 g/cm<sup>3</sup>. The plot gives  $1.0244 \pm 0.0001$  g/cm<sup>3</sup>, which is what would be expected. Also, equation 3 allows  $\rho_s$  to be accurately calculated from the tabulated values of  $W$ ,  $\phi$  and a pore fluid density of 1.0245 g/cm<sup>3</sup>. That is, equation 3 indicates that the relationships between  $\rho_s$ ,  $\phi$ ,  $W$  and  $\rho_p$  are correct.

The difference in the application of equations 1 and 3 is that equation 1 involves the use of the tabulated values of  $\rho_g$ , whereas equation 3 does not. Values of  $\rho_g$  back-calculated from equations 2 or 4 significantly differ from the tabulated values of  $\rho_g$  in a manner which seemed to indicate that there is an error associated with back-calculated

values of  $\rho$ , which is proportional to the porosity of the sample.

Relating these observations back to the measured parameters, there seemed to be no problem with the water content values, which are derived entirely from the weight determinations. There seems to be no problem with the tabulated or measured values of grain density, which are derived from the weight determinations and from the dry volume, but all the back-calculated values of grain density involve porosity or bulk density, which are derived from the weight determinations, the pore fluid density (assumed to be 1.0245 g/cm<sup>3</sup>) and the wet volume. It was therefore concluded that the measured values of wet volume, as determined by the Quantachrome helium Penta-Pycnometer, were in error and that consequently the tabulated values of porosity and bulk density presented in Proceedings of the Ocean Drilling Program - Initial Reports Volume 123 (1990) are also in error. These errors did not come to light during the periodic checks of the accuracy of the pycnometer because the calibration standards used were dry and not wet. It was subsequently confirmed by ODP staff at Texas A&M University that there was a "problem" with the pycnometer and that it had been known of for some time prior to Leg 123.

#### 4.2.2 Corrections to the Data

It is possible to rearrange the equations used for the determination of porosity and bulk density so that they do not utilise the measured values of wet volume. In this sense, the wet volume information is redundant although it does, if measured accurately, allow additional checks on data conformity.

By re-arranging equation 7 it can be shown that:

$$\phi = \frac{W \rho_g}{(W \rho_g + 1.0245)}$$

and by substituting this into 9;

$$\rho_s = 1.0245 \frac{\rho_g (W + 1)}{(W \rho_g + 1.0245)}$$

These two equations were therefore used to back-calculate corrected values of porosity and bulk density which would have been determined had there been no error in wet volume. The corrected data are presented in Table 1 for Site 765 and Table 2 for Site 766. Corrections were not applied to the basalt samples from Site 766, for which the original pycnometer derived data were no longer available.

It can also be shown that by re-arranging either of the two equations above, a plot of the corrected values against the measured values of porosity, or a plot of the corrected values against the measured values of bulk density, will yield a slope equal to the ratio of the measured value of wet volume over the value of wet volume which would have been obtained had there been no error. For each of these two plots the slope is  $0.938 \pm 0.001$ . That is, all measured values of porosity and bulk density were about 6.2% too high.

#### 4.3 Index Property Correlations

A frequency histogram of grain densities for all the sediment samples from Sites 765 and 766 is shown in Fig. 3. The data ranges from 2.16 to 3.22 g/cm<sup>3</sup> but the average is  $2.677 \pm 0.134$  g/cm<sup>3</sup> with a

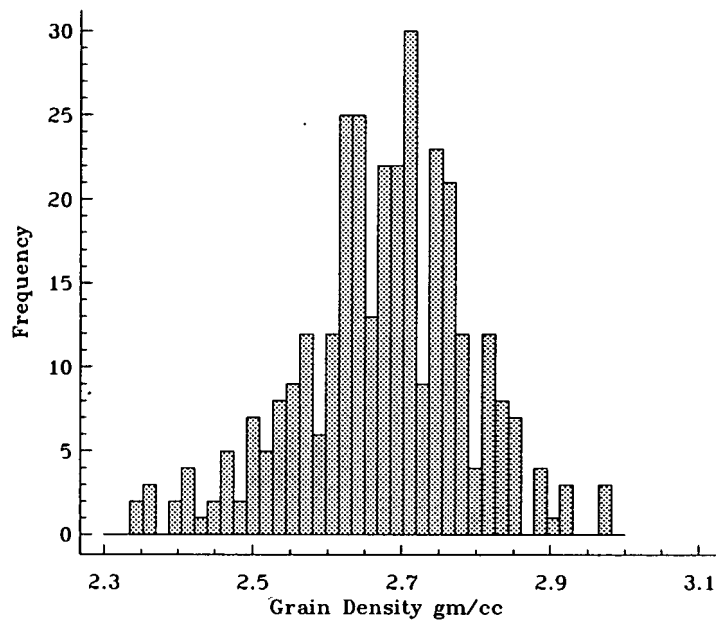


Figure 3 Histogram of Sediment Grain Densities

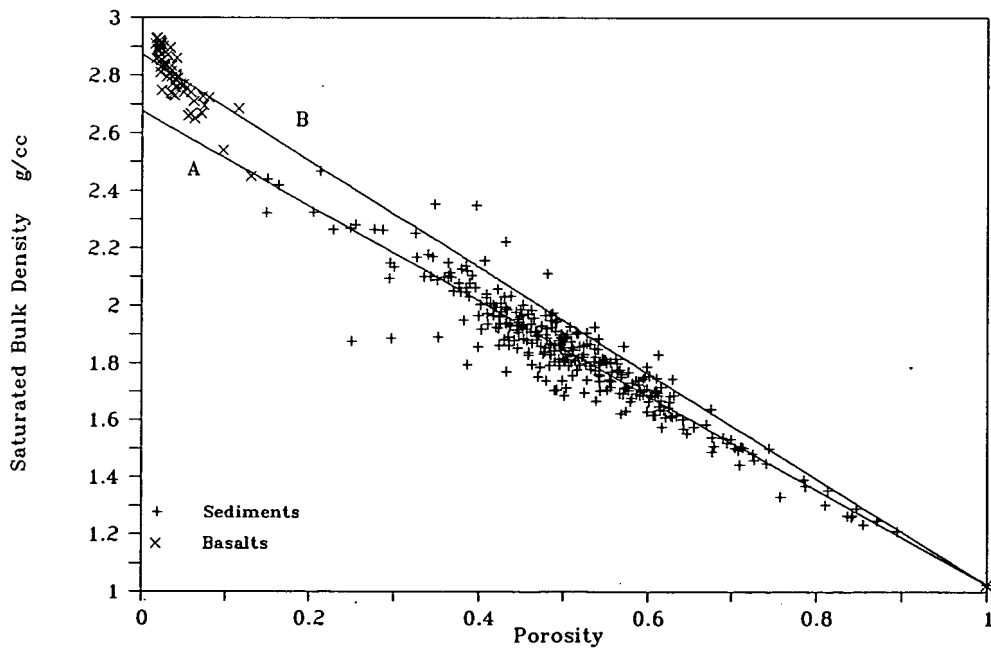


Figure 4 Porosity-Bulk Density Plots

geometric mean of 2.674 and a mode of 2.64. The cyclicity of the histogram suggests data groupings about grain density values of about 2.55, 2.64 (quartz), 2.71 (calcite), 2.75 and 2.82 g/cm<sup>3</sup> with the majority falling in the quartz-calcite range. Similarly, the data range of grain densities for all the basalt samples lies between 2.66 and 2.97 g/cm<sup>3</sup> with an average of 2.872 ± 0.064 g/cm<sup>3</sup>, a geometric mean of 2.871 and a mode of 2.85.

It was shown earlier that a plot of  $\rho_s$  against  $\phi$ , should yield an intercept of  $\rho_p$  and a slope of  $(\rho_p - \rho_g)$ . Such a plot for all the sediment and basalt samples is shown in Fig. 4. A linear regression through the sediments gives an equivalent grain density of 2.667 ± 0.017 g/cm<sup>3</sup>, a pore fluid density of 1.034 g/cm<sup>3</sup> (slope = -1.633 ± 0.032), with an R<sup>2</sup> of 88.9%. A similar regression through the basalts gives an equivalent grain density of 2.876 ± 0.008 g/cm<sup>3</sup>, a pore fluid density of 0.967 g/cm<sup>3</sup> (slope = -1.909 ± 0.063) with an R<sup>2</sup> of 93.9%. All of these data are well within the expected ranges. The two lines drawn through the data on Fig. 4 are based upon a pore fluid density of 1.0245 g/cm<sup>3</sup> and grain densities of 2.872 g/cm<sup>3</sup> and 2.677 g/cm<sup>3</sup> for the upper and lower lines respectively.

## 5 POROSITY - VELOCITY TRANSFORMS

### 5.1 Background

Ever since Wyllie et al (1956), the now famous Wyllie time average equation has been universally applied to predict porosities from compressional wave velocities, or visa-versa. The application of the equation has ranged from its routine use in the petrophysical analysis of geophysical borehole logs (Schlumberger, 1972; Dresser Atlas, 1982; Hearst and Nelson, 1985); to lithology and porosity determinations (Domenico, 1984); and algorithms for calculating depth-porosity relationships and understanding subsidence history (Stam et al, 1987).

In their paper Wyllie et al (1956) presented the time average equation in the form;

$$\frac{1}{v} = \frac{\phi}{v_p} + \frac{(1-\phi)}{v_g}$$

which can be rewritten more conveniently as;

$$\frac{1}{v} = \phi \left( \frac{1}{v_p} - \frac{1}{v_g} \right) + \frac{1}{v_g} \quad (10)$$

where  $v$  is the measured compressional wave velocity of the sample,  $v_p$  is the pore fluid velocity and  $v_g$  is the matrix velocity of the solid material. This equation, which is often presented in a modified form using travel times rather than velocities, represents a linear relationship between inverse velocity and porosity where the intercept, at  $\phi$  equals zero, is the inverse of the matrix velocity and where the pore fluid velocity can be determined from the slope. The equation was empirically derived from observations on synthetic aggregates of rigid media and produced a satisfactory fit to their data. A less satisfactory fit was observed when applied to rock materials (Wyllie et al, 1958), especially in the high porosity region. The poor fit to this, and other models discussed below, has been attributed to many factors in the subsequent literature including; increased sediment frame

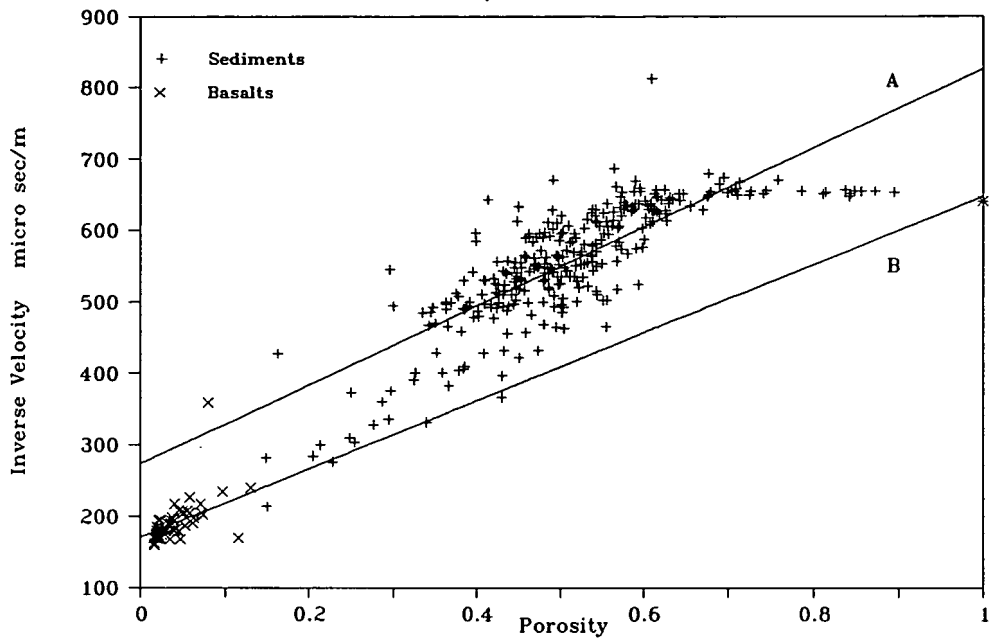


Figure 5 Wyllie Time Average Equation Plots

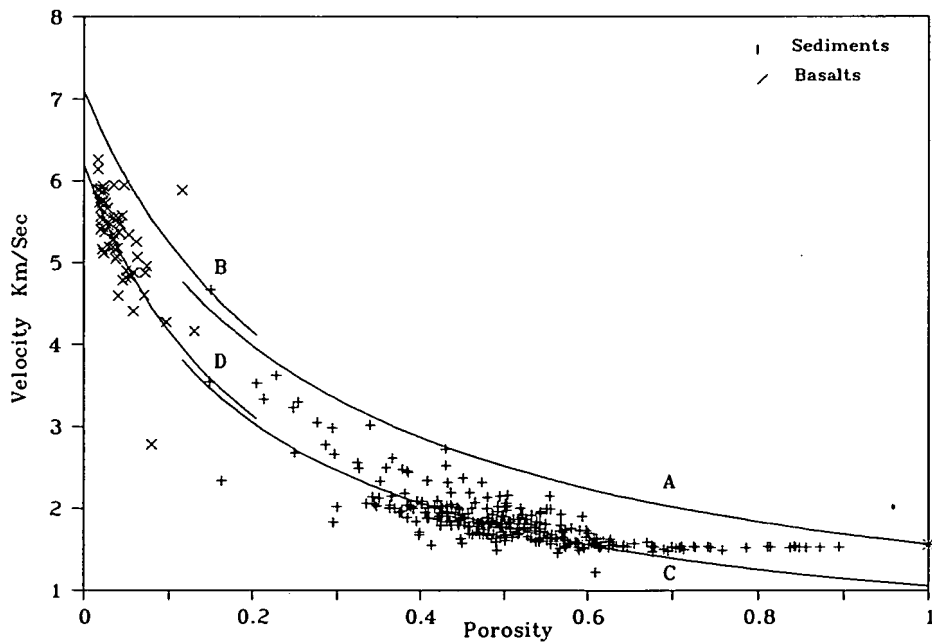


Figure 6 Wyllie Equation Predictions

bulk modulus and dynamic rigidity caused by overburden pressure, temperature and hydrostatic pressure effects (Fulthorpe and Schlanger, 1989; Gardner et al, 1974)

A plot of inverse velocity against porosity using the ODP Leg 123 data is shown in Fig. 5. Linear regression lines are drawn through each of the sediment and basalt data sets (lines A and B respectively) with no preconceived assumptions other than to include the water point (velocity = 1560 m/s in accordance with the equipment calibration - see section 2). Over the full porosity range the linearity of the data trend is not very convincing but within the range from 30 to 65% a satisfactory line could be drawn. Many porosity-velocity transform practitioners deal with somewhat amorphous clouds of data within this relatively narrow range, which probably explains why the Wyllie time average equation has been adhered to for so long. The levelling off of velocity above 65% porosity corresponds to the uncompactd calcareous ooze described in section 3.

A plot of velocity against porosity is shown in Fig. 6 upon which is superimposed plots of velocity derived from equation 10. For line A a  $v_p$  value of 6500 m/s for sediments was chosen as being intermediate between the quartz value of 6060 m/s and the calcite value of 6650 m/s (Yale, 1985). A  $v_p$  value for basalts (line B) of 7100 m/s was taken as being representative and in both cases a  $v_p$  value of 1560 m/s was used, as described above. It can be seen that these two lines do not pass through the data at all and that to force them to do so (lines C and D) requires the somewhat unrealistically low values of 5800, 6200 and 1050 m/s for the sediment and basalt matrix velocities and pore water velocity respectively.

It has long been recognized that the Wyllie equation does not adequately describe the actual relationship between velocity and porosity and there have been many attempts to circumvent these shortcomings. Yale (1985), in a comprehensive review of the literature, reported wide discrepancies between predicted and measured values of porosity. Han et al (1986) noted that the time average equation significantly overestimates velocities and found it necessary to use unrealistically low values of matrix velocity to accommodate a fit to the data.

Wilkins et al (1986) have used aspect ratio modelling to describe the effect of varying clay content on the porosity-velocity relationship; Castagna et al (1985), Han et al (1986), Taylor-Smith (1974), Anderson (1974) fitted least-squares empirical equations to their data to derive linear relationships between velocity, porosity and clay content; and Rafavich et al (1984) developed linear relationships involving a wide range of petrographic characteristics. The drawback to this sort of approach is that the coefficients derived to fit the empirical equations are specific to the rock materials for which they were determined, thereby limiting their applicability to particular formations and environments. Also there is often no physical basis to justify such equations.

An equally unsatisfactory approach, which is also of limited applicability, has been to modify the time average equation by applying a "compaction correction factor" to account for unconsolidated high porosity materials (Collins and Pilles, 1979; Schlumberger, 1972; Dresser Atlas, 1982). Anderson (1984) simulated the effect on velocity of oil and gas saturation but stressed that his theoretical model was only applicable under those conditions where the time average equation is satisfied.

Pioneering work in the field of the velocity of sound in porous media was carried out by Wood (1941) who showed that for a suspension

of solid particles in a liquid the mean bulk compressibility equals the sum of the compressibilities of the individual components. Since compressibility is the reciprocal of bulk modulus  $K$ , it follows that;

$$\frac{1}{K} = \frac{\phi}{K_p} + \frac{(1-\phi)}{K_g} \quad (11)$$

Also the fundamental equations governing velocity through a perfectly elastic, homogeneous, isotropic solid are given by;

$$\rho_s v_p^2 = K + \frac{4}{3}\mu$$

$$\rho_s v_s^2 = \mu$$

and

$$\sigma = \frac{(v_p^2/v_s^2 - 2)}{2(v_p^2/v_s^2 - 1)}$$

where  $\mu$  is the rigidity or shear modulus,  $v_p$  is the compressional wave velocity,  $v_s$  is the shear wave velocity and  $\sigma$  is Poisson's ratio. In the case of a suspension of solid particles in a liquid, the medium will lack rigidity,  $\mu$  becomes zero and therefore;

$$\frac{1}{\rho_s v^2} = \frac{\phi}{\rho_p v_p^2} + \frac{(1-\phi)}{\rho_g v_g^2} \quad (12)$$

Equation 12 is known as the Wood emulsion equation and can be written more conveniently as;

$$\frac{1}{\rho_s v^2} = \phi \left( \frac{1}{\rho_p v_p^2} - \frac{1}{\rho_g v_g^2} \right) + \frac{1}{\rho_g v_g^2} \quad (13)$$

Equation 13 represents a linear relationship between  $1/\rho_s v^2$  and porosity. A plot using the ODP Leg 123 data is shown in Fig. 7 with linear regression lines drawn through each of the sediment (line A) and basalt (line B) data sets under the same assumptions as for Fig. 5. The linearity of the data is a considerable improvement over the time average equation but there is a significant S shaped characteristic to the plot.

Hamilton (1971) and the McCanns (1968a and 1968b) have shown that while a suspension of solid particles in a liquid can, to a certain extent, be regarded as a two-phase medium, the Wood equation simply puts a lower limit on the magnitude of velocity (Buchan et al, 1971). This can be readily seen in the literature where the Wood equation has been fitted to data; Shumway (1960), Buchan et al (1971), Taylor-Smith (1974), Jackson et al (1981), and Nobes et al (1986). Indeed, Nobes et al (1986) found it necessary to take an empirically weighted mean of both the Wood and Wyllie equations to compute a better representation to their data over the full range of porosities of Pacific Ocean floor sediments.

To counteract this minimum limit effect Wyllie et al (1956)

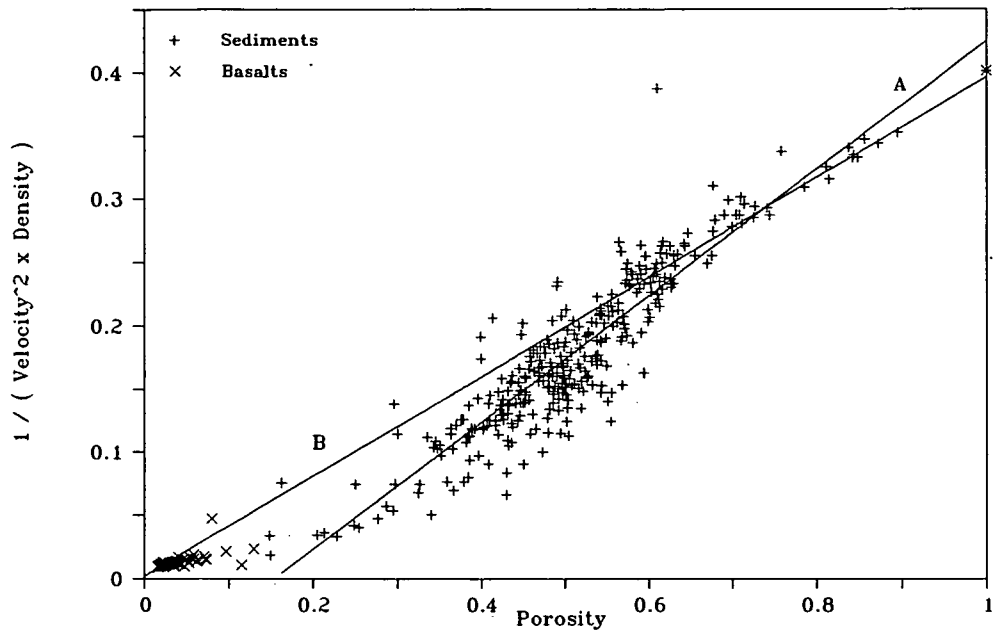


Figure 7 Wood Emulsion Equation Plots

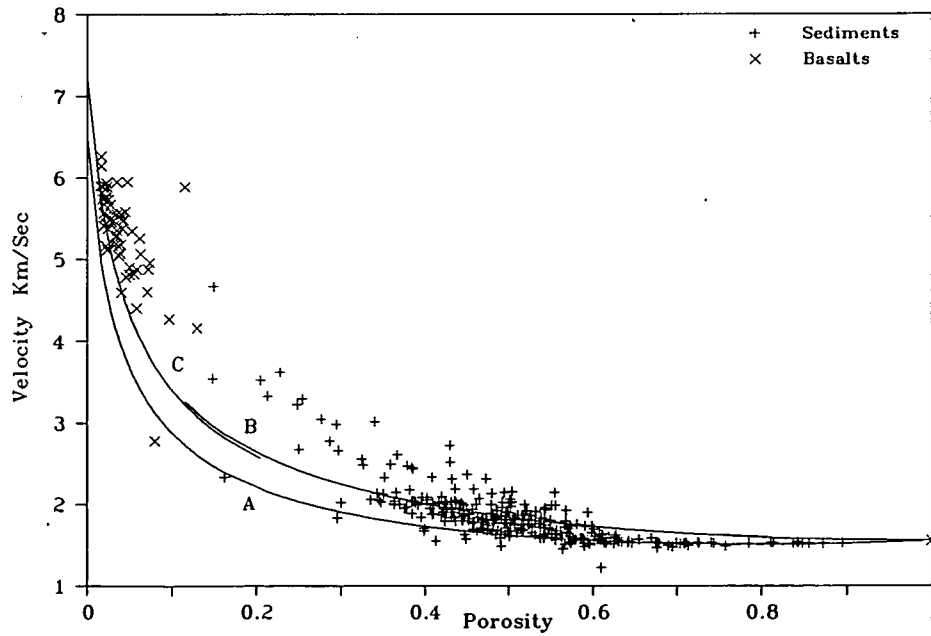


Figure 8 Wood Equation Predictions

introduced the rigidity of the bulk materials and solid matrix into the Wood equation giving the following (presented here in the form of equation 13);

$$\frac{(1+q)}{\rho_s v^2} = \phi \left( \frac{1}{\rho_p v_p^2} - \frac{(1+q_g)}{\rho_g v_g^2} \right) + \frac{(1+q_g)}{\rho_g v_g^2} \quad (14)$$

where

$$q = \frac{2(1-2\sigma)}{(1+\sigma)} \quad \text{and} \quad q_g = \frac{2(1-2\sigma_g)}{(1+\sigma_g)}$$

Jackson et al (1981) developed a similar argument but presented their equations in the form of compressibilities and the shear wave velocity of the bulk material. Laughton (1957) questioned the validity of equation 11 and argued that when a sediment has been subjected to ever increasing consolidation pressures over geological time, its rigidity increases. He introduced an extra factor to the bulk modulus,  $K_c$ , to allow for the resistance to deformation of the structure of the solid particles. His modified form of equation 11 then becomes;

$$\frac{1}{K - K_c} = \frac{\phi}{K_p} + \frac{(1-\phi)}{K_g}$$

Taking this into account the Wood equation becomes (in the form of equation 13);

$$\frac{1}{\rho_s v^2 - K_c} = \phi \left( \frac{1}{\rho_p v_p^2} - \frac{1}{\rho_g v_g^2} \right) + \frac{1}{\rho_g v_g^2} \quad (15)$$

On closer inspection however, because Laughton assumed that structure deformation consists only of shearing strains in the particles and inter-particle bonds, this equation can be seen to be the same as the Wyllie-Wood equation (14) except that the  $q_g$  term is missing.

An examination of the Laughton-Wood equation (15) reveals that it has the effect of increasing the entire range of predicted velocity values, including the matrix velocity and the pore water velocity, by an amount equal to  $(1+q)^{0.5}$ . This is more than 26% for a  $q$  value of 0.6 and is clearly not acceptable. The Wyllie-Wood equation has a similar effect at the high porosity end of the range but, if  $q$  and  $q_g$  are equal, the predicted velocity approaches the matrix velocity at the low end of the range. Clearly, neither Laughton nor Wyllie intended that the inclusion of shear modulus effects in the Wood equation should be applied with equal weight at both the high and low ends of the porosity range. Since the Wood equation was derived to describe loose suspensions of solid particles in a liquid, the inclusion of shear modulus effects should be at a minimum at the higher porosities, increasing progressively to a maximum at the lower porosities. This can be achieved by multiplying both  $q$  and  $q_g$  by  $(1-\phi)$  so that equation 14 becomes;

$$\frac{(1+q(1-\phi))}{\rho_s v^2} = \phi \left( \frac{1}{\rho_p v_p^2} - \frac{(1+q_g(1-\phi))}{\rho_g v_g^2} \right) + \frac{(1+q_g(1-\phi))}{\rho_g v_g^2} \quad (16)$$

A plot of velocity against porosity for the ODP Leg 123 data is shown in Fig. 8, upon which is superimposed a plot of sediment velocities

derived from the Wood equation (13), line A, using matrix and pore water velocities as before, a pore fluid density of 1.0245 g/cm<sup>3</sup>, and a grain density of 2.667 g/cm<sup>3</sup>. The bulk density values were derived from equation 6. Although the overall curvature of this line tends to represent a minimum envelope as described above, it actually plots *through* the data in the porosity range of about 62% to 100%, rather than below it. Therefore, in this porosity range the Wood equation predicts velocity very well.

Also shown in Fig. 8 is a plot of velocity predicted from the modified Wyllie-Wood equation (16) for the sediments (line B) and the basalts (line C). These are based upon; sediment parameters as for line A; a basalt matrix velocity of 7100 m/s and grain density of 2.872 g/cm<sup>3</sup>; a  $q_g$  value of 0.55 derived from a Poisson's ratio of 0.32 (from velocities given in Yale, 1985); and a mean bulk  $q$  value of 0.6 derived from a Poisson's ratio of 0.3 (Wyllie et al, 1956; Domenico, 1984). Lines B and C show good correlations between the predicted and measured velocities over most of the porosity range. With unequal values for  $q$  and  $q_g$ , however, the predicted velocities approach values other than the matrix velocities as the porosity approaches zero. In this case they are 6604 m/s and 7214 m/s for the sediments and basalts respectively.

Nafe and Drake (1957) took a slightly different approach to Wyllie et al (1956) and Laughton (1957) and considered the application of applied pressures to the total system. They made certain empirical assumptions and derived the following equation;

$$v = \phi v_*^2 \left( 1 + \frac{\rho_p}{\rho_s} (1 - \phi) \right) + \frac{\rho_g}{\rho_s} v_g^2 (1 - \phi)^n$$

where  $v_*$  is the velocity predicted by the Wood equation (13) and  $n$  was suggested to lie between 4 and 5. Nafe and Drake (1957) commented that comparison of their equation with experimental data gave velocities that are too low at the higher porosities and that this could not be improved by different choices of  $n$ . This observation is confirmed in Fig. 9 where line A is the prediction using the sediment parameters used previously and line B is the prediction using the basalt parameters. In both cases a value for  $n$  of 5.5 was needed to reach a moderately acceptable fit to the measured values of velocity from ODP Leg 123 data and even then the predicted values were, in general, too low over the 50 to 100% porosity range and too high over the 0 to 50% range. In order to produce a somewhat more acceptable match, it was necessary to use an unrealistically low matrix velocity of 5800 m/s, as shown in line C (the model is relatively insensitive to grain density variations).

More recently, in the development of porosity-velocity transforms, Raymer et al (1980) presented three algorithms to describe the upper and lower porosity ranges separately and a linear interpolation to link the two. The first two algorithms were given as alternatives for the 0 to 37% range and are;

$$v = \left( \frac{\rho_g}{\rho_s} \right)^{0.5} (1 - \phi)^{1.9} v_g \quad (17)$$

and

$$v = \phi v_p + (1 - \phi)^2 v_g \quad (18)$$

The third Raymer algorithm, to describe the 47 to 100% range, was stated

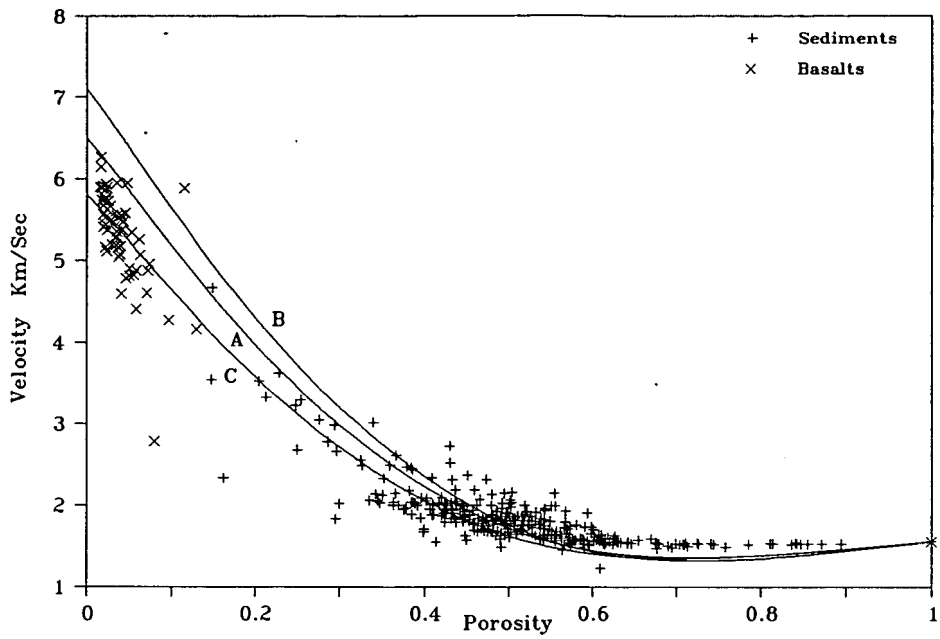


Figure 9 Nafe & Drake Equation Predictions

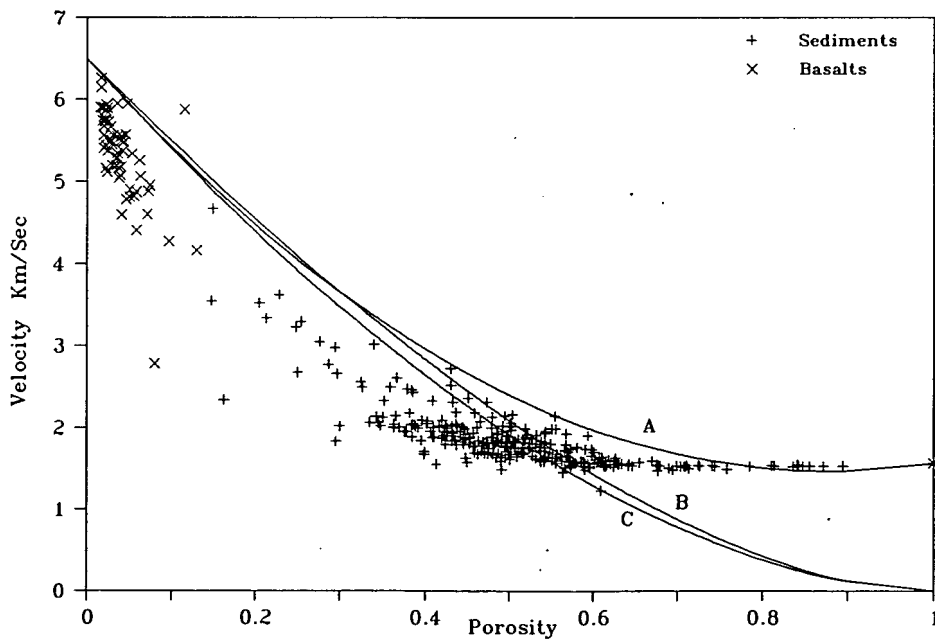


Figure 10 Raymer and Raiga-Clemenceau Equation Predictions

to be totally empirical but is in fact the Wood equation (though not attributed as such). Raiga-Clemenceau et al (1988) introduced the concept of acoustic formation factor to describe the velocity-porosity relationship in the 0 to 50% porosity range. Their empirically derived equation is of the form;

$$v = v_g(1 - \phi)^x \quad (19)$$

where the exponent x was taken to be 1.76 for a calcite matrix.

Velocities derived from equations 17 (line B), 18 (line A) and 19 (line C) are shown in Fig. 10 using the sediment parameters only: matrix velocity = 6500 m/s throughout; pore fluid velocity = 1560 m/s for line A; pore fluid density = 1.0245 g/cm<sup>3</sup>, grain density = 2.667 g/cm<sup>3</sup> and bulk density values derived from equation 6 for line B; and exponent x = 1.76 for line C. As claimed by Raymer et al (1980), lines A and B are virtually the same over the 0 to 37% porosity range while the Raiga-Clemenceau et al (1988) line C is almost the same as line B over the entire porosity range. The Raiga-Clemenceau et al (1988) algorithm does not, therefore, differ significantly from the Raymer et al (1980) algorithms and they all predict consistently higher velocities than those measured for the ODP Leg 123 samples, in much the same way as the Wyllie time average equation.

## 5.2 The Acoustic Impedance Transform

The well defined data relationship between porosity and velocity spawned much of the work discussed in the previous section. An equally well defined relationship between bulk density and velocity has also long been recognised, and the use of acoustic impedance (the product of velocity and bulk density) to determine reflection coefficients is an established tool in seismic interpretation (Rafavich et al, 1984). Gardner et al (1974) derived an empirical exponential relationship between density and velocity based upon reflection coefficient considerations. The close linearity between porosity and reflection coefficient is relatively well documented (Buchan et al, 1971; Taylor-Smith, 1974) but does not seem to have been explored as the basis of a potential porosity-velocity transform.

Following the lead given by Wood and Wyllie, a plot of inverse acoustic impedance against porosity is shown in Fig. 11 using the ODP Leg 123 data, with linear regression lines drawn through each of the sediment (line A) and basalt (line B) data sets under the same assumptions as for Fig. 5. The linearity of the data is clear and is significantly better than that for the Wood equation (Fig. 7). These linear regression lines are represented by the following equation;

$$\frac{1}{\rho_s v} = \phi \left( \frac{1}{\rho_p v_p} - \frac{1}{\rho_g v_g} \right) + \frac{1}{\rho_g v_g} \quad (20)$$

Figure 12 shows a plot of velocities derived from equation 20 (line A) superimposed upon the Leg 123 velocity-porosity data using the same sediment parameters as before. For direct comparison, the velocities derived from the Wood equation (13), previously shown as Line A, Fig. 8, are also shown in Fig. 12. It is clear that while the original Wood equation is a better predictor of velocities over the 45 to 100% porosity range, equation 20 predicts the velocities more closely over the 0 to 45% porosity range. Indeed, over the entire porosity range, equation 20 tends to represent a closer approximation to a minimum envelope to the data than has been postulated for the Wood equation.

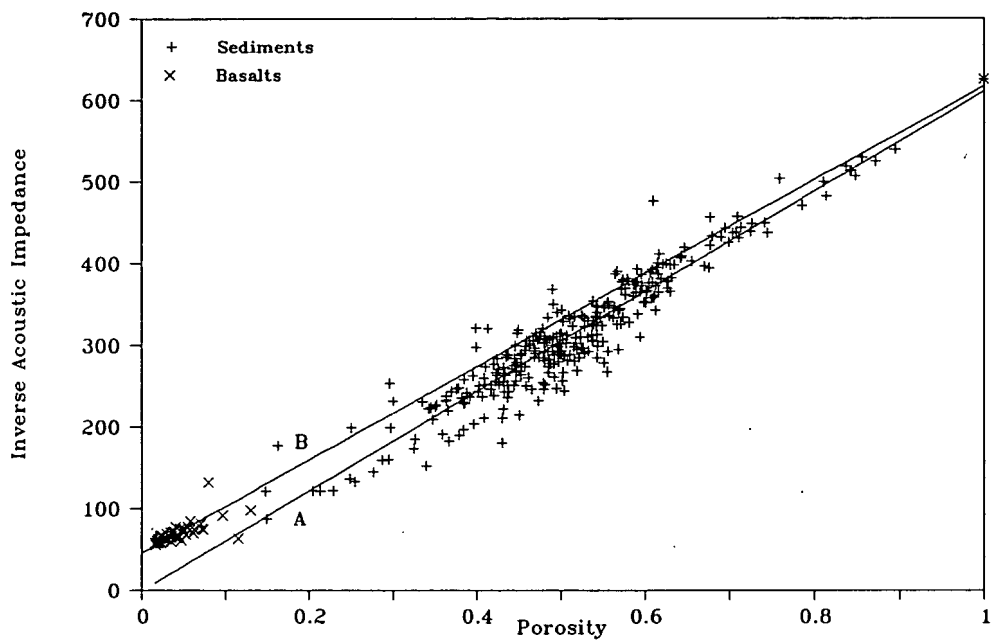


Figure 11 Acoustic Impedance Equation Plots

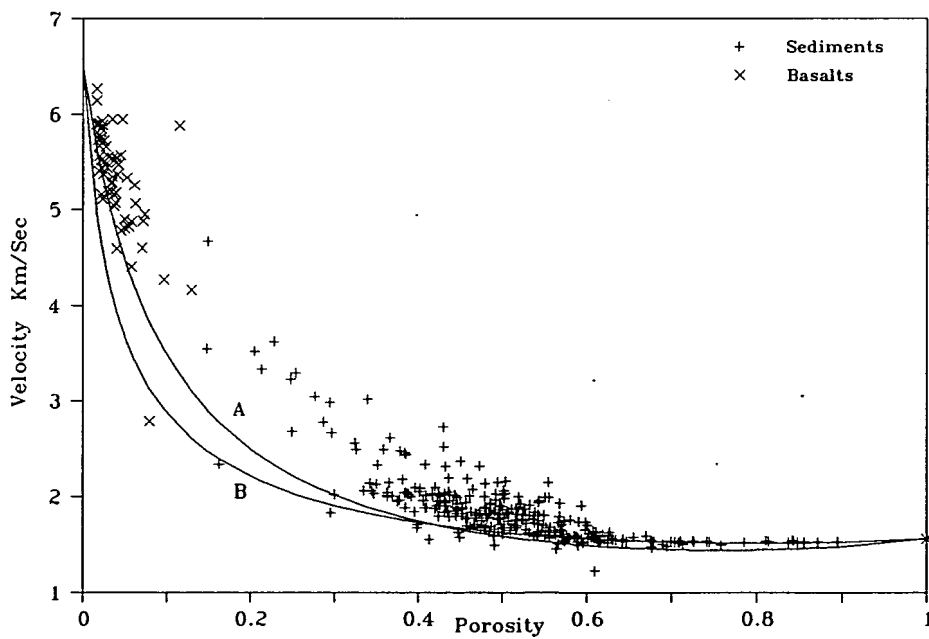


Figure 12 Acoustic Impedance and Wood Equation Predictions

Following a similar line of argument to that which led to the development of equation 16, equation 20 can be modified in the following way;

$$\frac{(1+q(1-\phi))}{\rho_s v} = \phi \left( \frac{1}{\rho_p v_p} - \frac{(1+q_g(1-\phi))}{\rho_g v_g} \right) + \frac{(1+q_g(1-\phi))}{\rho_g v_g} \quad (21)$$

This is a semi-empirical equation based in part upon the fully validated concepts of acoustic impedance. When the velocities predicted by this equation are compared to the ODP Leg 123 data, using the same parameters as used in Fig. 8, (ie; a sediment matrix velocity of 6500 m/s, a sediment grain density of 2.667 g/cm<sup>3</sup>, a basalt matrix velocity of 7100 m/s, a basalt grain density of 2.872 g/cm<sup>3</sup>, a pore water velocity of 1560 m/s, a pore fluid density of 1.0245 g/cm<sup>3</sup>, and bulk density values derived from equation 1) they tend to be a little too high over the higher porosity range. However, adjusting  $q$  and  $q_g$  to be both equal to 0.22 (equivalent to a Poisson's ratio of 0.42) results in lines A and B shown in Fig. 13 for the sediments and basalts respectively.

The velocity values predicted by the acoustic impedance equation above, achieve a very much closer fit to the measured values of velocity than those predicted by the modified Wyllie-Wood equation over both the upper and lower porosity ranges. The adjustment to the  $q$  values in the acoustic impedance equation is considered acceptable because of the semi-empirical nature of equation 21, but a Poisson's ratio of 0.42 is still within the range of values presented in the literature for limestones and sandstones. A similar adjustment to the  $q$  values used in the modified Wyllie-Wood equation may be less acceptable, because of the firm basis of this equation in elasticity theory, but if the  $q$  values used in equation 16 are both reduced to 0.45 (equivalent to a Poisson's ratio of 0.35) then a better fit to the data can be achieved. Even so this fit is still not as close as that represented by lines A and B in Fig. 13.

A more accurate representation of predicted velocities for individual samples will, of course, be obtained by using the measured values of grain density and bulk density rather than derived values of bulk density from equation 6 and average grain densities. This procedure does not, however, give smooth curves for the purposes of comparing the velocity predictions of one model against another. As a measure of the correlation between the predicted and measured values of velocity, the values derived from equations 16 and 21 were re-calculated using the measured grain and bulk densities for each sample. A linear regression equation was then calculated for the predicted velocities, derived from each of the acoustic impedance and the modified Wyllie-Wood equations, against the measured values of velocity. A perfect correlation would result in a slope of 1, an intercept of 0 and an R<sup>2</sup> of 100. The values for the acoustic impedance equation were 0.90 ± 0.01, 144 ± 250 and 96 respectively and those for the modified Wyllie-Wood equation were 0.70 ± 0.01, 455 ± 245 and 95.

## 6 THERMAL CONDUCTIVITY RELATIONSHIPS

All the thermal conductivity values determined during the Leg 123 cruise are listed in Tables 3 and 4 for Sites 765 and 766 respectively.

Although it was not practicable to measure thermal conductivities and index properties on the same sample, it has been possible to compare predictive equations by assuming that each thermal conductivity sample would have similar index properties to the closest depth match index

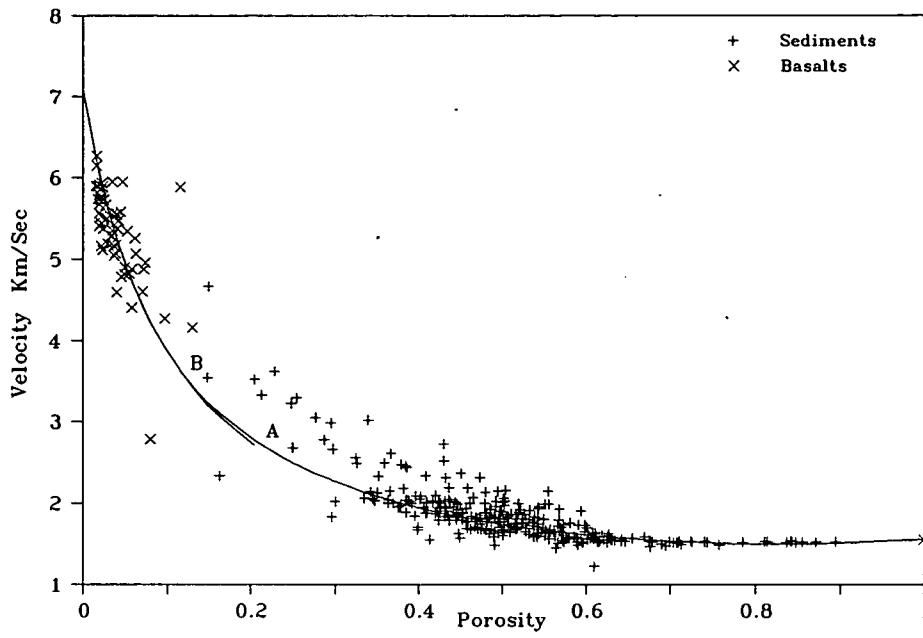


Figure 13 Modified Acoustic Impedance Equation Predictions

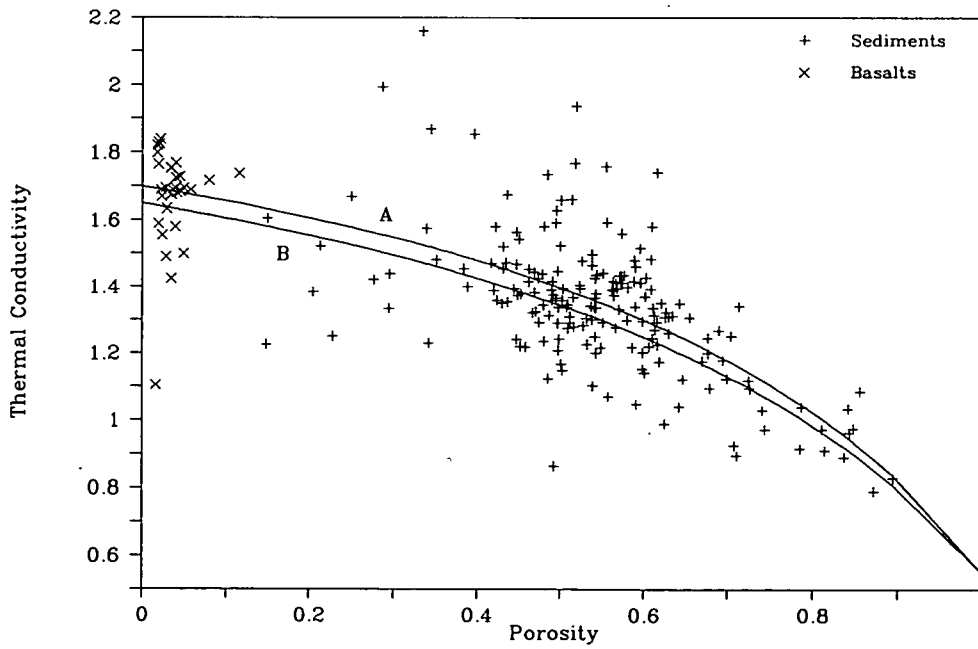


Figure 14 Thermal Conductivity Predicted From Equation 22

property sample. Clearly this will introduce correlation errors, but depth mis-matches averaged only 0.8 m between the two sets of core samples.

It has been shown in earlier sections of this report that satisfactory models describing relationships between porosity and other physical properties such as bulk density, bulk modulus, and velocity are all of the general form;

$$f_s = f_p \phi + f_g (1 - \phi)$$

Where  $f$  is an appropriate function. By following a similar line of reasoning, a convincing relationship between thermal conductivity and porosity can be shown to be of the form;

$$\kappa \rho_s = \phi (\kappa_p \rho_p) + (1 - \phi) \kappa_g \rho_g \quad (22)$$

where  $\kappa$  is the thermal conductivity of the sample,  $\kappa_p$  is the pore fluid thermal conductivity, and  $\kappa_g$  is the rock matrix thermal conductivity. Satisfactory correlations between predictions and measured values (Fig. 14) can be obtained by using basalt matrix and sediment matrix thermal conductivities of 1.70 and 1.65 W/m °C respectively (lines A and B) and a pore fluid value of 0.55 W/m °C.

Nobes et al (1986), however, used a relationship of the following form to derive thermal conductivities from porosity;

$$\kappa = \kappa_p^\phi \kappa_g^{(1-\phi)} \quad (23)$$

Again, reasonably satisfactory correlations between predictions and measured values (Fig. 15) can be achieved by using corresponding matrix and pore fluid thermal conductivities of 1.75, 2.60 and 0.70 W/m °C respectively

The spread of measured values of thermal conductivity as porosity decreases, due in part to the lack of correspondence between the samples, leads to difficulties when deciding which of these two models is most appropriate. However, physical considerations would lead one to expect that thermal conductivity, porosity and density express some degree of interdependence and that equation 22 might be the more realistic. Also by plotting the linearised forms of these two relationships, equation 22 produces a marginally more convincing straight line than does equation 23.

## 7 DISCUSSION AND CONCLUSIONS

The limitations of the Wyllie time average equation have been known for many years and have been re-emphasised here by comparing predicted and measured compressional wave velocities of marine samples ranging from oozes, close to the sea-sediment interface, through to basement basalts.

Some of the limitations of the time average equation were also recognised by Wyllie and his co-workers who amended the Wood emulsion equation to partially take account of the rigidity of the materials. Further modifications to this Wyllie-Wood equation have been shown here to not only describe the relationship between porosity and velocity more closely than the time average equation, but also more closely than some of the alternative proposals suggested by contemporaries of Wyllie and since. Indeed, bearing in mind the Wyllie-Wood equation was discussed

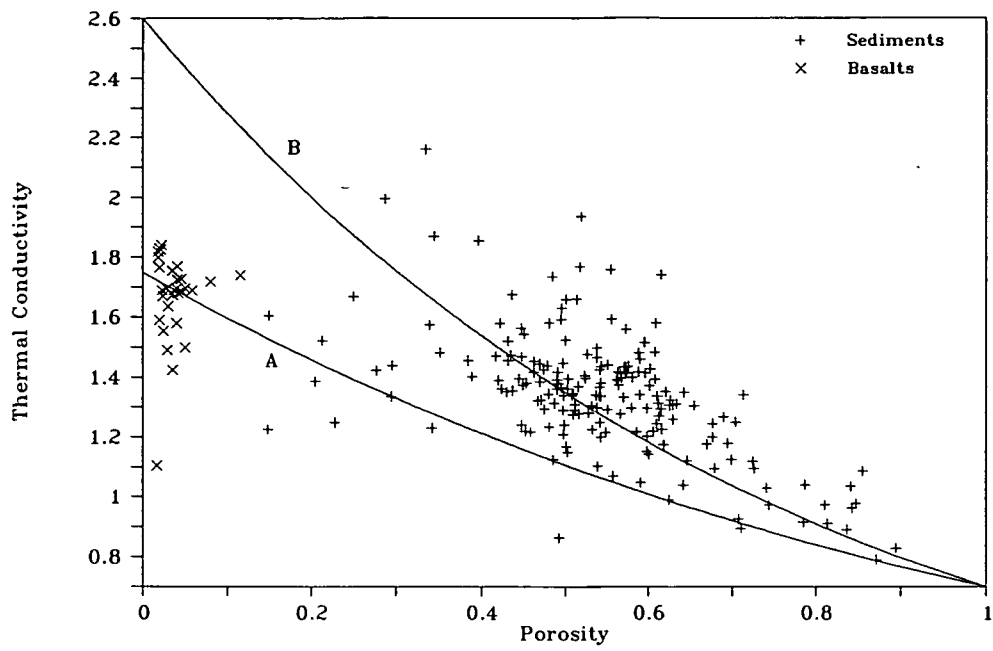


Figure 15 Thermal Conductivity Predicted From Equation 23

in the same paper the time average equation was first proposed, it is somewhat curious that the time average equation has been adhered to for so long. Furthermore, it is curious that some of the more recent publications do not seem to take account of, or even be aware of, the pioneering research carried out in this field in the 1950's.

A semi-empirical acoustic impedance relationship has been developed which is shown to provide a more accurate porosity-velocity transform, using realistic material parameters, than has hitherto been possible. The fact that a closer correlation can be achieved with this semi-empirical equation, than with the more theoretically based modified Wyllie-Wood equation, perhaps opens to question some of the fundamental assumptions governing compressibilities of materials upon which this early work was based.

It has also been shown that a satisfactory empirical equation can be used to describe the relationships between thermal conductivity and porosity. The lack of direct correspondence between measured samples has, however, precluded this relationship being explored in more detail.

If enough is known about the lithology to provide estimates of the matrix and pore water parameters, equations 6, 21 and 22 enable a complete description of the behaviour of a saturated rock core in terms of compressional wave velocity, thermal conductivity, porosity and bulk density. If measurements of bulk density and grain density are also available then it allows average values of some of these parameters to be determined or alternatively removes the necessity of assuming grain densities for each sample.

## 8 ACKNOWLEDGEMENTS

I wish to thank Michael Riggins, my fellow Physical Properties Specialist during Leg 123; Roland Beaussillon who performed many of the thermal conductivity determinations; John Ludden and Felix Gradstein, the two Co-Chief Scientists; Andrew Adamson, the ODP Staff Scientist; and all the scientific party and crew of JOIDES Resolution during the cruise.

## 9 REFERENCES

Anderson, R. A., 1984. Fluid and frequency effects on sonic velocities. SPWLA Trans., 25<sup>th</sup> Logging Symposium, Paper AAA.

Anderson, R. S., 1974. Statistical correlation of physical properties and sound velocity in sediments. In: Hampton, L., Ed. Physics of Sound in Marine Sediments. Plenum Press, New York and London.

Boyce, R. E., 1976. Definition and laboratory techniques of compressional sound velocity parameters and wet-water content, wet-bulk density, and porosity parameters by gravimetric and gamma ray attenuation techniques. In Shlanger, S.O., Jackson, E.D., et.al., Init. Repts. DSDP, 33: Washington (U.S. Govt. Printing Office), pp.931-958.

Buchan, S., Dewes, F. C. D., Jones, A. S. G., McCann, D. M., and Taylor-Smith, D., 1971. The acoustic and geotechnical properties of North Atlantic cores. University College of North Wales, Marine Science Laboratories, Geological Report 71-1.

Castagna, J. P., Batzle, M. L. and Eastwood, R. L., 1985. Relationships between compressional-wave and shear-wave velocities in clastic silicate rocks. Geophysics, 50 (4), pp.571-581.

Collins, H. N., and Pilles, D., 1979. Some uses of functional analysis in petrophysics. 7th Formation Evaluation Symposium of the Canadian Well Logging Society.

Domenico, S. N., 1984. Rock lithology and porosity determinations from shear and compressional wave velocity. *Geophysics*, 49 (8), pp.1188-1195.

Dresser Atlas. 1982. Well logging and interpretation techniques.

Fulthorpe, C. S., and Schlanger, S. O., 1989. In situ acoustic properties of pelagic carbonate sediments on the Ontong Java Plateau. *J. Geophys. Res.*, 94, pp.4025-4032.

Gardner, G. H. F., Gardner, L. W., and Gregory, A. R., 1974. Formation velocity and density - the diagnostic basics for stratigraphic traps. *Geophysics*, 39 (6), pp.770-780.

Hamilton, E. L., 1971. Elastic properties of marine sediments. *J. Geophys. Res.*, 76 (2), pp.579-604.

Hamilton, E. L., 1974. Prediction of deep-sea sediment properties: state-of-the-art. In: Inderbitzen, A. L., Ed. *Deep-sea sediments*. Plenum Press, New York and London.

Han, D., Nur, A., and Morgan, D., 1986. Effects of porosity and clay content on wave velocities in sandstone. *Geophysics*, 51 (11), pp.2093-2107.

Hearst, J. R., and Nelson, P. H., 1985. *Well logging for physical properties*. McGraw-Hill.

Jackson, P. D., Baria, R., and McCann, D. M., 1981. Geotechnical assessment of superficial marine sediments using in-situ geophysical probes. *Ocean Management*, 7, pp.189-209.

Laughton, A. S., 1957. Sound propagation in compacted ocean sediments. *Geophysics*, 22 (2), pp.233-260.

McCann, C., 1968a. An investigation of the acoustic properties of natural materials. Unpubl. PhD Thesis, University of Wales, Bangor.

McCann, D. M., 1968b. The acoustic properties of North Atlantic cores. Unpubl. PhD Thesis, University of Wales, Bangor.

Nafe, J. E., and Drake, C. L., 1957. Variation with depth in shallow and deep water marine sediments of porosity, density and the velocities of compressional and shear waves. *Geophysics*, 22 (3), pp.523-552.

Nobes, D. C., Villinger, H., Davis, E. E., and Law, L. K., 1986. Estimation of marine sediment bulk physical properties at depth from seafloor geophysical measurements. *J. Geophys. Res.*, 91, pp.14033-14043.

ODP Leg 123 shipboard scientific party. 1989a. *Ocean Drilling Program - the birth of the Indian Ocean*. *Nature*, 337 (9 February), pp.506-507.

ODP Leg 123 shipboard scientific party. 1989b. ODP investigates Indian Ocean origins. *Geotimes* 34 (3), pp.16-19.

ODP Leg 123 shipboard scientific party. 1990. *Proceedings of the Ocean Drilling Program - Initial Reports. Vol 123 - Argo Abyssal Plain and the Gascoyne Abyssal Plain. Sites 765-766, September - November, 1988*. National Science Foundation. Joint Oceanographic Institutions, Inc. [in press].

Rafavich, F., Kendall, C. H. St. C., and Todd, T. P., 1984. The relationship between acoustic properties and the petrographic character of carbonate rocks. *Geophysics*, 49 (10), pp.1622-1636.

Raiga-Clemenceau, J., Martin, J. P., and Nicoletis, S., 1988. The concept of acoustic formation factor for more accurate porosity determination from sonic transit time data. *The Log Analyst*, Jan-Feb, 1988.

Raymer, L. L., Hunt, E. R., and Gardner, J. S., 1980. An improved sonic transit time-to-porosity transform. *SPWLA Trans.*, 21<sup>st</sup> Logging Symposium, Paper P.

Schlumberger. 1972. *Log interpretation principles*.

Shumway, G., 1960. Sound and absorption studies of marine sediments by a resonance method, parts I and II. *Geophysics*, 25, (2) pp.451-467, and (3) pp.659-682.

Stam, B., Gradstein, F. M., Lloyd, P., and Gillis, D., 1987. Algorithms for porosity and subsidence history. *Computers and Geosciences*, 13 (4), pp.317-349.

Taylor-Smith, D., 1974. Acoustic and mechanical loading of marine sediments. In: Hampton, L., Ed. *Physics of sound in marine sediments*. Plenum Press, New York and London.

Vacquier, V., 1985, The measurement of thermal conductivity of solids with a transient linear heat source on the plane surface of a poorly conducting body, *Earth Planet, Sci. Lett.*, 74, pp.275-279.

Von Herzen, R. P. and Maxwell, A. E., 1959. The measurement of thermal conductivity of deep-sea sediments by a needle probe method. *J. Geophys. Res.*, 65, pp1557-1563.

Wilkins, R. H., Simmons, G., Wissler, T. M. and Caruso, L., 1986. The physical properties of a set of sandstones - part III. The effects of fine-grained pore filling material on compressional wave velocity. *Int. J. Rock Mech. Min. Sci. & Geomech. Abstr.* 23 (4), pp.313-325.

Wood, A. B., 1941. *A textbook of sound*. The Macmillan Company, New York.

Wyllie, M. R. J., Gregory, A. R., and Gardner, L. W., 1956. Elastic wave velocities in heterogeneous and porous media. *Geophysics*, 21 (1), pp.41-70.

Wyllie, M. R. J., Gregory, A. R., and Gardner, G. H. F., 1958. An experimental investigation of factors affecting elastic wave velocities in porous media. *Geophysics*, 23 (3), pp.459-493.

Yale, D. P., 1985. Recent advances in rock physics. *Geophysics*, 50 (12), pp.2480-2491.

TABLE 1  
Index and Velocity Values for Site 765

SAMPLE ID				DEPTH mbsf	BULK DENSITY g/cm <sup>3</sup>	GRAIN DENSITY g/cm <sup>3</sup>	POROSITY %	WATER CONTENT %	VELOCITY m/s
<i>Sediments</i>									
A	1H	2	78	2.28	1.33	2.29	75.8	139.8	1491
A	1H	4	68	5.18	1.25	2.76	87.2	252.2	1526
A	1H	6	68	8.18	1.44	2.46	70.9	101.4	1516
B	1H	1	96	0.96	1.21	2.79	89.4	311.2	1530
B	1H	3	42	3.42	1.29	2.77	84.7	205.0	1525
B	1H	6	61	8.11	1.23	2.48	85.5	244.5	1527
B	2H	1	53	9.83	1.50	2.88	74.4	103.3	1523
B	2H	3	65	12.95	1.30	2.50	81.1	175.7	1535
B	2H	6	75	17.55	1.35	2.79	81.4	160.4	1530
B	3H	1	83	19.63	1.45	2.66	74.1	110.0	1534
B	3H	4	125	24.55	1.26	2.51	84.1	216.3	1544
B	3H	6	22	26.52	1.51	2.69	71.0	93.4	1537
B	4H	2	98	30.98	1.48	2.68	72.4	100.3	1537
B	4H	4	115	34.15	1.39	2.73	78.5	137.0	1524
B	4H	6	90	36.90	1.27	2.56	84.3	214.1	1535
B	5H	1	119	39.29	1.27	2.50	83.7	209.8	1522
B	5H	4	127	43.87	1.46	2.61	72.6	103.9	1526
B	6H	2	102	50.32	1.49	2.63	70.7	94.2	1525
B	6H	4	55	52.85	1.37	2.64	78.7	143.2	
B	7H	1	113	58.53	1.52	2.65	69.5	88.0	1482
B	7H	4	65	62.55	1.64	2.67	62.4	63.8	1521
B	7H	6	37	65.27	1.57	2.55	64.3	72.3	1556
B	8H	2	49	69.09	1.53	2.71	69.9	87.7	1531
B	8H	5	42	73.52	1.55	2.52	64.6	74.3	1534
B	8H	6	107	75.67	1.57	2.46	61.7	67.0	1543
B	9H	2	77	79.07	1.50	2.69	71.3	94.6	1498
B	9H	3	67	80.47	1.61	2.61	63.0	66.7	1557
B	9H	6	36	84.66	1.54	2.62	67.6	81.7	1537
B	10H	1	98	87.38	1.58	2.62	65.5	74.1	1575
B	10H	2	77	88.67	1.58	2.72	67.0	76.3	1590
B	10H	6	87	94.77	1.63	2.62	61.9	63.4	1603
B	11H	1	62	96.62	1.60	2.64	64.2	69.7	1534
B	11H	3	92	99.92	1.67	2.70	61.5	60.7	1547
B	11H	5	59	102.59	1.68	2.79	62.7	61.6	1604
B	12H	2	117	108.27	1.64	2.92	67.5	73.0	1545
B	12H	3	77	109.37	1.69	2.82	63.1	62.1	1547
B	12H	5	78	112.38	1.62	2.64	63.4	67.2	1552
B	13H	3	115	119.35	1.61	2.57	62.1	65.3	1554
B	13H	5	133	122.53	1.68	2.58	58.0	54.8	1573
B	13H	6	77	123.47	1.74	2.75	58.6	52.7	1592
B	14H	1	76	125.56	1.69	2.71	60.5	57.9	1572
B	14H	4	79	130.09	1.67	2.55	57.9	55.2	1571
B	14H	5	68	131.48	1.70	2.75	60.8	57.7	1640
B	15H	1	100	135.50	1.76	2.86	60.2	54.1	1558
B	15H	4	84	139.84	1.69	2.64	59.0	55.8	1568
B	15H	6	104	143.04	1.68	2.68	60.3	58.0	1618
B	16H	1	28	144.48	1.66	2.73	62.6	62.7	1591
B	16H	3	80	148.00	1.62	2.54	60.9	62.7	1574
B	16H	6	50	152.20	1.62	2.53	60.6	62.3	1586
B	17H	1	68	154.58	1.71	2.63	57.2	52.0	1580
B	17H	4	80	159.20	1.75	2.80	59.4	53.5	1567

Table 1 - 1

B	18H	2	47	165.57	1.75	2.97	62.9	58.6	1565
B	18H	4	97	168.47	1.63	2.45	57.3	56.2	1609
B	18H	6	134	171.84	1.75	2.88	61.0	55.7	1593
B	19X	1	40	173.70	1.64	2.62	61.5	62.5	1522
B	19X	2	67	175.47	1.69	2.73	61.2	59.3	1588
B	19X	4	123	179.03	1.85	2.82	54.1	42.8	1610
B	20X	3	112	187.12	1.85	2.66	49.8	38.2	
B	20X	4	87	188.37	1.83	2.72	52.4	41.5	
B	20X	5	90	189.90	1.70	2.75	61.1	58.6	
B	21X	1	67	193.37	1.70	2.63	57.6	53.0	1586
B	21X	2	60	194.80	1.77	2.78	57.6	50.1	1562
B	21X	3	137	197.07	1.80	2.80	56.3	47.2	1596
B	22X	2	80	204.70	1.69	2.64	58.6	55.0	1577
B	22X	3	87	206.27	1.80	2.76	55.1	45.6	1601
B	22X	4	60	207.50	1.83	2.67	51.2	40.2	
B	23X	1	31	212.41	1.78	2.65	53.8	45.0	1588
B	23X	2	40	214.00	1.71	2.36	49.0	41.7	1590
B	24X	1	64	222.44	1.76	2.63	54.1	46.0	1628
B	24X	2	128	224.58	1.79	2.93	59.9	52.3	
B	24X	4	85	227.15	1.80	2.61	50.9	40.7	1648
B	25X	1	50	232.00	1.87	2.81	52.8	40.8	1657
B	26X	2	102	243.72	1.87	2.82	53.1	41.2	1624
B	26X	3	13	244.33	1.90	2.85	51.8	38.6	1695
B	27X	1	48	251.38	1.93	2.75	47.5	33.7	1679
B	27X	3	64	254.54	1.81	2.61	50.3	39.7	1674
B	28X	1	20	260.80	1.90	2.68	47.1	34.0	1691
B	28X	2	90	263.00	1.76	2.63	54.3	46.2	1637
B	29X	1	87	271.07	1.78	2.75	56.4	48.1	1626
B	30X	1	35	280.25	1.69	2.72	60.8	58.5	1568
B	31X	2	79	291.89	1.84	2.59	47.9	36.3	1693
B	31X	4	10	294.20	1.91	2.85	51.6	38.3	1755
B	32X	1	45	299.75	1.89	2.76	50.1	37.2	1679
B	32X	3	29	302.59	1.91	2.69	46.7	33.4	1711
B	33X	1	111	310.11	1.94	2.83	49.1	34.9	1660
B	33X	4	84	314.34	1.92	2.78	48.7	35.0	1688
B	34X	1	89	319.59	1.92	2.75	48.1	34.5	1673
B	34X	1	98	319.68	1.92	2.75	48.1	34.5	
B	35X	1	110	329.40	1.98	2.81	46.3	31.4	1679
B	36X	2	40	339.80	1.94	2.69	44.8	30.9	1631
B	37X	1	42	347.92	1.97	2.77	45.8	31.3	1696
B	37X	CC	56	350.43	2.06	2.71	38.4	23.6	2460
B	38X	1	103	358.13	1.94	2.72	46.2	32.4	1688
B	38X	CC	10	358.70	1.89	2.76	50.2	37.4	2062
B	39X	1	32	367.02	1.83	2.64	50.4	39.5	
C	2R	1	80	360.40	1.99	2.72	43.2	28.6	1839
C	2R	3	47	363.07	2.25	2.84	32.4	17.3	2559
C	3R	1	25	369.55	1.86	2.76	51.9	40.1	1998
C	3R	1	111	370.41	1.93	2.66	44.5	30.9	1823
C	3R	2	25	371.05	1.85	2.52	44.6	32.7	1799
C	3R	2	40	371.20	1.82	2.69	52.1	41.5	1923
C	4R	1	35	379.35	1.86	2.67	49.0	36.9	1830
C	4R	1	118	380.18	2.28	2.71	25.4	12.9	3296
C	4R	2	84	381.34	1.89	2.76	50.3	37.5	1980
C	4R	3	58	382.58	2.10	2.66	34.2	20.0	2141
C	5R	1	78	389.38	1.95	2.85	49.2	34.8	1845
C	5R	3	28	391.88	1.89	2.66	46.9	34.0	1779
C	5R	3	78	392.38	1.89	2.78	50.4	37.5	2161
C	6R	1	89	399.19	2.06	2.81	42.2	26.6	1903
C	6R	3	34	401.64	1.75	2.40	47.0	37.9	1814
C	6R	3	45	401.75	1.83	2.66	50.7	39.6	1746

Table 1 - 2

C	6R	3	70	402.00	2.03	2.72	40.8	26.0	2336
C	7R	1	109	409.09	1.93	2.64	43.7	30.1	1793
C	7R	2	106	410.56	2.27	2.68	24.8	12.6	3228
C	7R	3	34	411.34	1.83	2.57	47.7	36.3	1747
C	8R	1	49	418.19	1.88	2.72	49.6	37.0	1766
C	8R	2	133	420.53	2.26	2.63	22.8	11.5	3624
C	8R	3	22	420.92	1.85	2.71	51.2	39.6	
C	8R	4	22	422.42					2134
C	8R	4	71	422.91	1.94	2.57	41.0	27.7	1886
C	9R	1	59	427.89	1.74	2.63	55.5	48.5	2148
C	9R	2	112	429.92	1.78	2.58	51.6	42.4	1679
C	9R	3	40	430.70	2.09	2.54	29.4	16.8	2979
C	9R	5	60	433.90	1.76	2.52	51.1	42.5	1714
C	10R	2	30	438.30	1.72	2.58	55.5	49.6	1990
C	10R	2	47	438.47	1.96	2.65	42.4	28.5	1796
C	10R	4	33	441.33	1.87	2.71	49.7	37.4	1906
C	10R	4	112	442.12					1650
C	11R	1	111	447.11	1.89	2.60	45.4	32.7	1825
C	11R	2	91	448.41	2.26	2.76	28.6	14.9	2776
C	11R	3	110	450.10	2.13	2.80	37.9	22.3	2475
C	11R	4	116	451.66	1.62	2.61	62.7	66.0	1629
C	12R	1	68	455.88	1.96	2.77	46.5	32.2	2075
C	12R	3	85	459.05	2.10	2.72	36.3	21.5	2040
C	12R	4	36	460.06	2.05	2.69	38.5	23.8	1887
C	12R	5	67	461.87	1.93	2.63	43.7	30.2	2193
C	13R	1	96	465.56	2.44	2.69	15.0	6.7	4670
C	13R	2	127	467.37	2.08	2.75	38.9	23.7	2021
C	13R	3	10	467.70	1.91	2.67	46.2	32.9	2003
C	14R	1	59	474.69	1.99	2.73	43.2	28.5	1958
C	15R	1	17	483.87	1.71	2.64	57.4	52.2	1741
C	16R	1	103	494.23	2.11	3.12	48.2	30.5	1879
C	16R	2	24	494.94					1871
C	16R	4	50	498.20	2.35	3.06	34.7	17.8	2031
C	17R	1	133	503.73	1.93	2.67	45.2	31.7	1800
C	17R	2	109	504.99	1.84	2.63	48.9	37.3	
C	17R	3	40	505.80	2.04	2.74	40.8	25.8	1882
C	18R	1	78	512.68	1.86	2.51	43.6	31.5	1854
C	18R	2	48	513.88	1.81	2.64	51.4	41.0	1708
C	18R	3	40	515.30	1.99	2.72	43.3	28.8	1907
C	19R	1	55	521.85	1.87	2.66	48.5	36.2	1827
C	19R	2	81	523.61	1.91	2.89	52.8	39.6	1808
C	19R	3	119	525.49	1.94	2.65	43.6	29.9	2048
C	20R	1	50	531.30	2.03	2.67	38.8	24.3	2033
C	20R	1	94	531.74	2.14	2.83	38.3	22.5	2039
C	20R	2	71	533.01	1.79	2.47	47.3	37.2	1823
C	21R	1	15	540.55	2.11	2.80	39.1	23.5	2000
C	22R	1	61	550.71	1.87	2.60	46.3	34.0	
C	22R	1	148	551.58	2.05	2.65	36.9	22.6	2004
C	22R	2	102	552.62	1.81	2.56	49.0	38.5	1842
C	23R	4	3	564.23	2.13	2.61	30.0	16.8	2023
C	23R	5	3	565.73	2.10	2.64	33.4	19.5	2063
C	24R	1	40	569.70	2.15	2.79	36.3	20.9	2010
C	24R	1	146	570.76	2.10	2.71	36.3	21.5	2001
C	24R	3	4	572.34	2.35	3.22	39.6	20.9	2091
C	25R	1	37	579.37	2.17	2.77	34.4	19.4	2059
C	25R	3	62	582.62	2.08	2.71	37.5	22.7	1952
C	25R	5	19	585.19	2.05	2.67	37.8	23.3	1968
C	26R	4	34	593.04	1.76	2.73	56.9	49.5	1655
C	26R	5	37	594.12	1.71	2.55	55.2	49.5	1677
C	27R	1	45	597.95	1.70	2.75	61.1	58.5	1632

Table 1 - 3

C	27R	2	18	599.25	1.74	2.63	55.7	48.9	1650
C	28R	1	85	607.85	1.77	2.71	55.7	47.6	1680
C	28R	2	97	609.47	1.81	2.71	53.6	43.7	1771
C	29R	1	82	617.22	1.83	2.65	50.3	39.1	1775
C	29R	5	35	622.97	1.82	2.59	49.5	38.7	1769
C	29R	6	10	624.27	1.88	2.76	50.9	38.5	
C	30R	2	56	627.95	1.88	2.73	49.8	37.2	1781
C	30R	4	107	631.39	1.74	2.58	54.3	47.1	1753
C	30R	6	80	634.09	1.90	2.84	51.6	38.5	1868
C	31R	1	3	635.33	2.32	2.55	14.8	7.0	3549
C	31R	2	74	637.45	1.93	2.67	44.8	31.1	1863
C	31R	3	138	639.56	1.93	2.69	45.3	31.6	1882
C	32R	1	77	645.77	1.96	2.72	44.8	30.6	1848
C	35R	1	127	675.37	1.79	2.51	48.4	38.3	1823
C	35R	2	94	676.54	1.83	2.59	48.6	37.4	1933
C	35R	3	78	677.88	1.74	2.40	48.0	39.4	1890
C	35R	4	41	679.01	1.80	2.46	46.3	35.9	1841
C	36R	2	10	684.90	1.77	2.34	43.3	33.4	2315
C	36R	5	120	690.50	1.84	2.53	45.9	34.4	1777
C	36R	6	45	691.25	1.86	2.41	39.9	28.2	1676
C	37R	1	107	694.07	1.70	2.51	54.4	48.6	1959
C	37R	2	62	695.12	2.00	2.81	45.2	30.1	1888
C	37R	3	96	696.96	1.93	2.58	42.0	28.8	1876
C	38R	1	142	703.92	1.92	2.58	42.3	29.1	1949
C	38R	3	47	705.97	1.80	2.28	38.6	28.2	2438
C	38R	5	104	709.54	1.86	2.48	42.4	30.4	2035
C	38R	7	7	711.57	1.88	2.60	45.7	33.2	1938
C	39R	1	82	712.52	1.91	2.62	44.7	31.6	1876
C	39R	3	51	715.21	1.71	2.41	50.3	43.1	2031
C	40R	2	124	723.64	1.97	2.64	41.7	27.8	2017
C	40R	4	22	725.62	1.90	2.79	50.5	37.4	1823
C	41R	1	9	730.49	2.01	2.70	41.3	26.7	1553
C	42R	1	46	740.26	1.86	2.62	47.9	36.0	1888
C	42R	2	15	741.45	1.99	2.77	45.0	30.2	1578
C	42R	4	59	744.89	1.91	2.77	49.1	35.7	1491
C	43R	2	121	751.81	1.86	2.72	50.9	39.1	
C	43R	4	138	754.98	1.86	2.63	48.2	36.3	1776
C	43R	6	52	757.12	1.90	2.77	49.8	36.7	1808
C	44R	2	91	760.91	1.85	2.81	53.7	42.3	1762
C	44R	4	34	763.34	2.42	2.69	16.3	7.4	2338
C	45R	1	92	769.12	1.91	2.69	46.9	33.6	1829
C	45R	5	70	774.90	1.89	2.69	48.1	35.3	1806
C	46R	1	41	778.21	1.89	2.75	49.8	36.9	1772
C	46R	2	36	779.66	1.97	2.86	48.5	33.8	1850
C	47R	1	112	788.52	1.92	2.75	48.1	34.5	1848
C	47R	4	32	792.22	1.92	2.67	45.7	32.3	1770
C	48R	1	86	797.76	2.22	3.13	43.1	24.8	2028
C	48R	6	127	805.67	2.01	2.74	42.6	27.8	1957
C	49R	1	98	807.28	1.94	2.61	42.5	29.0	1907
C	49R	4	82	811.62	1.94	2.64	43.4	29.7	1938
C	50R	2	90	818.00	1.94	2.63	43.2	29.6	1941
C	50R	5	38	821.98	2.16	2.93	40.6	23.9	1957
C	51R	1	35	825.35	1.93	2.67	45.0	31.4	1929
C	51R	5	5	831.05	2.00	2.66	40.1	25.8	2053
C	52R	2	12	836.12	2.03	2.82	43.8	28.3	2023
C	52R	3	102	838.52	1.98	2.74	44.4	29.9	2013
C	53R	1	29	844.39	1.88	2.53	43.0	30.6	2520
C	53R	4	26	848.86	2.17	2.72	32.6	18.2	2492
C	53R	7	37	853.47	1.92	2.52	40.3	27.4	2084
C	54R	1	109	854.59	2.00	2.70	41.7	27.1	2029

Table 1 - 4

C	54R	4	90	858.90	1.95	2.52	38.2	25.1	2181
C	55R	1	107	864.07	1.95	2.70	44.6	30.6	1991
C	55R	3	82	866.82	2.12	2.81	38.6	22.9	2044
C	56R	1	67	873.17	2.00	2.70	42.0	27.5	2097
C	56R	2	94	874.94	1.98	2.69	42.6	28.3	2003
C	57R	1	6	881.76	1.94	2.68	44.7	30.9	1923
C	57R	3	69	885.39	2.11	2.74	36.5	21.5	2147
C	58R	1	90	892.10	2.09	2.66	35.0	20.7	2129
C	58R	4	40	896.10	1.97	2.63	40.9	27.0	2010
<i>Basalts</i>									
C	63R	2	23	937.47	2.75	2.85	5.3	2.0	5341
C	63R	4	133	941.54	2.76	2.85	4.8	1.8	5952
C	64R	1	48	945.78	2.65	2.76	6.3	2.5	5067
C	65R	1	27	954.97	2.86	2.89	1.7	0.6	6267
C	65R	2	40	956.50	2.71	2.82	6.2	2.4	5260
D	1R	1	113	949.03	2.77	2.85	4.5	1.7	5578
D	2R	2	31	956.40	2.93	2.96	1.7	0.6	6148
D	2R	3	88	958.04	2.75	2.79	2.4	0.9	5893
D	3R	1	35	964.75	2.79	2.86	4.0	1.5	5495
D	5R	1	16	983.36	2.80	2.86	3.5	1.3	5552
D	5R	1	118	984.38	2.83	2.90	3.5	1.3	5952
D	5R	5	61	988.77	2.81	2.88	3.5	1.3	5292
D	6R	2	30	994.20	2.72	2.87	8.0	3.1	2785
D	7R	1	138	1003.38	2.92	2.96	2.3	0.8	5936
D	7R	2	122	1004.68	2.70	2.83	7.4	2.9	4955
D	7R	3	48	1005.36	2.73	2.86	7.2	2.8	4883
D	8R	1	37	1011.87	2.80	2.88	4.0	1.5	5550
D	9R	1	38	1021.28	2.83	2.87	2.2	0.8	5859
D	9R	3	17	1024.01	2.87	2.93	3.0	1.1	5563
D	10R	1	116	1031.36	2.76	2.83	4.0	1.5	5551
D	11R	1	45	1039.85	2.88	2.92	2.0	0.7	5792
D	12R	1	55	1045.65	2.73	2.80	3.7	1.4	5160
D	13R	1	18	1054.58	2.73	2.80	3.9	1.5	5073
D	14R	1	9	1063.99	2.89	2.93	2.0	0.7	5410
D	15R	2	26	1074.76	2.83	2.88	2.5	0.9	5377
D	16R	1	58	1083.08	2.81	2.85	2.2	0.8	5528
D	17R	3	13	1094.67	2.77	2.86	5.0	1.9	4903
D	18R	1	99	1102.09	2.90	2.94	2.0	0.7	5907
D	18R	3	78	1103.92	2.77	2.84	3.7	1.4	5041
D	19R	1	98	1111.28	2.74	2.83	5.0	1.9	4814
D	19R	2	38	1111.98	2.79	2.87	4.3	1.6	5481
D	20R	1	47	1119.97	2.80	2.85	3.0	1.1	5194
D	21R	1	86	1129.86	2.74	2.80	3.4	1.3	5193
D	22R	1	96	1139.56	2.67	2.77	5.9	2.3	4406
D	23R	2	65	1149.95	2.80	2.87	4.0	1.5	4598
D	24R	1	13	1157.23	2.83	2.88	2.7	1.0	5669
D	24R	3	33	1160.00	2.90	2.96	3.4	1.2	5284
D	24R	4	95	1161.85	2.68	2.90	11.5	4.6	5883
D	25R	2	11	1168.04	2.86	2.90	1.9	0.7	5675
D	26R	1	28	1176.28	2.83	2.90	3.5	1.3	5349

Table 1 - 5

TABLE 2  
Index and Velocity Values for Site 766

SAMPLE ID				DEPTH mbsf	BULK DENSITY g/cm <sup>3</sup>	GRAIN DENSITY g/cm <sup>3</sup>	POROSITY %	WATER CONTENT %	VELOCITY m/s
<i>Sediments</i>									
A	1R	2	30	1.80	1.50	2.64	70.4	92.3	1521
A	1R	3	39	3.39	1.51	2.53	67.9	85.5	1529
A	2R	2	60	9.86	1.54	2.68	69.0	84.9	1503
A	2R	7	21	16.97	1.49	2.46	67.6	87.0	1471
A	3R	1	10	17.40	1.65	2.64	61.3	61.5	1534
A	3R	4	35	22.15	1.80	2.78	55.6	46.1	1568
A	4R	1	129	28.29	1.71	2.71	59.6	55.7	1515
A	4R	2	105	29.55	1.77	2.74	56.4	48.4	1455
A	5R	2	97	39.17	1.74	2.76	58.9	53.2	1525
A	5R	5	70	43.40	1.71	2.63	57.2	52.1	1544
A	7R	4	56	61.06	1.75	2.83	59.6	53.5	1526
A	7R	6	118	64.68	1.72	2.65	57.4	52.1	1528
A	8R	1	50	66.20	1.69	2.57	56.7	52.1	1510
A	9R	1	47	75.77	1.73	2.73	58.9	53.7	1587
A	9R	4	94	80.74	1.70	2.68	59.0	55.1	1492
A	11R	1	133	96.03	1.79	2.55	49.6	39.5	1637
A	11R	4	51	99.71	1.83	2.59	48.5	37.2	1634
A	12R	1	35	104.65	1.81	2.59	50.1	39.7	1611
A	13R	2	13	115.53	1.71	2.82	61.6	58.2	1595
A	13R	3	116	118.06	1.74	2.64	55.4	48.3	1631
A	14R	2	50	125.60	1.86	2.97	57.1	45.9	1647
A	14R	4	120	129.30	1.82	2.77	54.7	44.6	1649
A	15R	6	20	140.90	1.71	2.77	61.0	57.8	1230
A	16R	1	52	143.42	1.83	3.10	61.2	52.2	1592
A	16R	3	67	146.57	1.88	2.90	54.1	41.7	1589
A	16R	5	43	149.33	1.93	2.97	53.7	40.0	1601
A	17R	2	106	155.06	1.80	2.72	54.3	44.8	1633
A	17R	5	111	159.61	1.82	2.83	56.2	46.4	1647
A	18R	2	146	165.06	1.78	2.76	56.6	48.5	1727
A	18R	4	14	166.74	1.74	2.54	52.8	45.1	1723
A	18R	6	33	169.93	1.90	2.67	47.0	34.0	1811
A	19R	1	38	172.08	1.75	2.71	56.8	49.7	1930
A	19R	3	131	176.01	1.79	2.70	54.1	44.8	1719
A	19R	5	21	177.91	1.81	2.76	54.9	45.1	1704
A	20R	1	17	181.57	1.93	2.74	47.4	33.7	1817
A	20R	3	11	184.51	2.15	2.62	29.5	16.4	1834
A	21R	1	16	191.16	1.89	2.56	43.5	30.8	1846
A	21R	2	90	193.40	1.88	2.64	46.9	34.3	1806
A	22R	1	25	200.85	1.89	2.25	29.7	19.2	2664
A	23R	1	29	210.59	1.88	2.56	44.2	31.7	1957
A	24R	1	53	220.43	1.92	2.63	44.5	31.2	1893
A	24R	CC	10	221.50	1.88	2.16	25.0	15.8	2679
A	25R	1	72	230.32	1.89	2.36	35.1	23.5	2332
A	26R	1	109	240.39	1.78	2.64	53.2	44.2	1915
A	26R	3	35	242.65	1.69	2.35	50.1	43.8	2017
A	27R	1	134	250.24	1.71	2.37	49.3	42.0	2028
A	27R	2	74	251.14	1.67	2.42	53.9	49.5	1838
A	28R	2	78	260.88	1.74	2.45	49.9	41.6	1901
A	28R	4	83	263.93	1.69	2.58	57.0	52.7	1711
A	28R	6	68	266.78	1.62	2.41	56.8	55.8	1793
A	29R	1	71	269.01	1.67	2.63	60.1	58.6	1702

A	29R	3	126	272.56	1.63	2.54	59.9	60.3	1734
A	30R	1	12	278.02	1.70	2.68	59.1	55.3	1737
A	30R	4	18	282.58	1.71	2.73	59.8	55.9	1656
A	31R	1	99	288.49	1.96	2.59	39.9	26.3	1708
A	32R	1	27	297.47	1.70	2.44	52.5	46.4	1751
A	32R	3	3	300.23	1.83	2.51	45.9	34.6	2186
A	32R	5	32	303.52	1.79	2.58	50.6	40.7	1840
A	33R	1	66	307.46	1.95	2.84	49.2	35.0	1964
A	33R	3	9	309.88	2.06	2.74	39.5	24.4	1844
A	34R	1	18	316.68	1.86	2.69	50.1	38.2	1867
A	34R	1	136	317.86	1.81	2.78	55.0	45.0	1807
A	36R	2	17	337.47	1.73	2.71	58.1	52.4	1760
A	37R	2	129	348.21	1.80	2.66	52.6	42.8	1870
A	37R	3	18	348.60	2.10	2.70	35.8	21.2	2493
A	38R	1	81	355.91	2.18	2.77	33.9	19.0	3017
A	38R	3	29	358.39	1.97	2.74	45.1	30.7	2369
A	39R	2	44	366.74	2.03	2.79	43.0	27.7	2727
A	39R	3	40	368.20	1.80	2.73	54.3	44.5	1940
A	40R	2	42	376.42	1.69	2.66	59.4	56.3	1906
A	40R	4	14	379.14	1.86	2.61	47.3	35.3	2317
A	41R	1	95	385.15	1.90	2.71	48.0	34.9	2135
A	41R	3	39	387.59	1.75	2.62	54.3	46.4	1817
A	41R	5	89	391.09	1.82	2.67	51.8	41.2	1816
A	42R	1	102	394.82	1.80	2.75	55.1	45.7	1991
A	42R	3	109	397.89	2.33	2.66	20.4	9.9	3523
A	43R	1	50	404.00	2.10	2.72	36.7	21.8	2613
A	43R	1	65	404.15	1.82	2.75	53.8	43.4	1797
A	43R	3	48	406.98	1.88	2.72	49.5	36.9	2150
A	43R	5	53	410.03	1.85	2.67	49.6	37.8	1866
A	44R	1	90	414.10	1.78	2.65	53.8	45.0	1728
A	44R	3	98	417.18	1.86	2.70	49.8	37.7	1707
A	44R	6	53	421.23	1.89	2.74	49.7	37.0	1773
A	45R	1	112	423.92	1.85	2.72	51.1	39.4	1868
A	45R	3	36	426.16	2.47	2.86	21.3	9.7	3337
A	45R	5	29	429.09	1.96	2.83	47.9	33.3	2000
A	46R	2	48	434.52	1.82	2.70	52.4	41.7	1766
A	46R	4	23	437.27	2.27	2.74	27.7	14.3	3050
A	46R	6	110	441.14	1.79	2.66	53.2	43.8	1801
A	47R	1	121	443.41	1.93	2.86	50.8	37.0	1840
A	47R	4	53	447.23	1.86	2.78	52.4	40.6	1809
A	48R	1	98	452.78	1.95	2.82	48.6	34.3	1921
A	48R	3	36	455.16	1.82	2.61	50.0	39.2	1901
A	48R	5	78	458.58	1.79	2.62	52.0	42.3	1890
<i>Basalts</i>									
A	48R	7	8	460.70	2.45	2.66	13.0	5.7	4161
A	48R	7	61	461.23	2.67	2.80	7.1	2.8	4603
A	49R	1	25	461.75	2.76	2.84	4.0	1.5	5179
A	49R	1	78	462.28	2.54	2.71	9.7	4.1	4270
<i>Sediments</i>									
A	49R	2	50	463.50	1.93	2.67	45.2	31.7	1874
A	49R	3	65	465.15	1.97	2.88	48.8	33.9	1822
<i>Basalts</i>									
A	49R	4	116	467.16	2.84	2.89	2.9	1.0	5451
A	49R	5	38	467.83	2.85	2.90	2.2	0.8	5439
A	50R	1	135	472.55	2.66	2.76	5.5	2.1	4821
A	50R	3	112	475.14	2.77	2.85	4.6	1.7	4787
A	50R	4	13	475.52	2.74	2.85	5.8	2.2	4877
A	51R	1	90	481.30	2.84	2.89	2.6	0.9	5515
A	51R	5	17	486.38	2.86	2.94	4.1	1.5	5372
A	52R	1	25	490.15	2.88	2.93	2.8	1.0	5498

Table 2 - 2

A	52R	3	98	493.95	2.89	2.92	1.8	0.6	5740
A	52R	5	55	496.29	2.90	2.95	2.2	0.8	5162
A	53R	1	35	499.45	2.90	2.93	2.0	0.7	5567
A	53R	3	52	502.22	2.91	2.95	2.1	0.7	5757
A	53R	5	62	504.51	2.90	2.95	2.5	0.9	5730
A	53R	7	91	507.60	2.91	2.96	2.4	0.9	5117
A	54R	2	108	510.70	2.91	2.94	1.6	0.6	5901
A	54R	4	96	513.22	2.93	2.97	1.8	0.6	5898
A	54R	6	118	515.68	2.92	2.96	2.1	0.8	5730

Table 2 - 3

TABLE 3  
Thermal Conductivity Values for Site 765

SAMPLE ID				DEPTH mbsf	Thermal Conductivity W/m °C
<i>Sediments</i>					
A	1H	2	40	1.50	0.812
A	1H	3	40	3.00	1.064
A	1H	4	40	4.50	0.791
A	1H	5	40	6.00	1.118
B	1H	1	40	0.00	0.777
B	1H	2	40	1.50	0.846
B	1H	3	40	3.00	0.892
B	1H	5	40	6.00	1.054
B	2H	1	40	9.30	0.973
B	2H	3	40	12.30	0.973
B	2H	5	40	15.30	0.874
B	2H	6	40	16.80	0.911
B	3H	1	40	18.80	1.030
B	3H	2	40	20.30	0.896
B	3H	3	40	21.80	0.837
B	3H	4	40	23.30	1.035
B	4H	1	50	28.50	0.895
B	4H	3	50	31.50	1.118
B	4H	4	50	33.00	0.916
B	4H	6	50	36.00	0.963
B	5H	1	40	38.10	0.891
B	5H	3	40	41.10	1.115
B	5H	5	40	44.10	1.095
B	5H	6	40	45.60	1.151
B	6H	1	40	47.80	1.053
B	6H	2	40	49.30	1.213
B	6H	3	40	50.80	0.926
B	6H	3	40	50.80	0.926
B	6H	6	40	55.30	1.040
B	7H	1	40	57.40	1.126
B	7H	3	40	60.40	1.231
B	7H	4	40	61.90	0.990
B	7H	6	40	64.90	1.350
B	8H	2	40	68.60	1.125
B	8H	4	40	71.60	1.123
B	8H	5	40	73.10	1.122
B	9H	1	45	76.80	1.225
B	9H	3	45	79.80	1.341
B	9H	4	45	81.30	1.259
B	9H	6	45	84.30	1.245
B	10H	1	40	86.40	1.306
B	10H	3	40	89.40	1.176
B	10H	5	40	92.40	1.328
B	10H	6	40	93.90	1.174
B	11H	1	40	96.00	1.041
B	11H	3	40	99.00	1.293
B	11H	5	40	102.00	1.362
B	11H	6	40	103.50	1.283
B	13H	1	60	115.20	1.312
B	13H	3	60	118.20	1.351
B	13H	5	60	121.20	1.199

B	13H	6	60	122.70	1.298
B	15H	1	51	134.50	1.371
B	15H	3	51	137.50	1.372
B	15H	5	51	140.50	1.340
B	15H	6	51	142.00	1.428
B	16H	2	50	145.70	1.307
B	16H	3	50	147.20	1.393
B	16H	5	50	150.20	1.242
B	16H	6	50	151.70	1.219
B	18H	2	50	165.10	1.278
B	18H	3	50	166.00	1.337
B	18H	5	50	169.00	1.433
B	18H	7	50	172.00	1.244
B	19X	2	30	174.80	1.375
B	19X	3	30	176.30	1.250
B	19X	4	30	177.80	2.146
B	19X	5	30	179.30	1.337
B	20X	2	37	184.50	1.113
B	20X	3	37	186.00	1.338
B	20X	5	37	189.00	1.396
B	20X	6	37	190.50	1.337
B	21X	2	50	194.20	1.435
B	21X	3	50	195.70	1.276
B	21X	4	50	197.20	1.414
B	21X	5	50	198.70	1.363
B	22X	1	36	202.40	1.428
B	22X	3	36	205.40	1.217
B	22X	4	36	206.90	1.441
B	22X	5	36	208.40	1.290
B	23X	1	110	212.10	1.480
B	23X	1	30	212.10	1.513
B	23X	2	110	213.60	1.318
B	23X	2	30	213.60	1.466
B	24X	1	40	221.80	1.425
B	24X	2	40	223.30	1.401
B	24X	3	40	224.80	1.296
B	24X	4	40	226.30	1.346
B	25X	1	50	231.50	1.282
B	26X	1	50	241.20	1.304
B	26X	3	50	244.20	1.768
B	26X	4	50	245.70	1.431
B	27X	1	30	250.90	1.325
B	27X	2	30	252.40	1.260
B	27X	3	50	253.90	1.430
B	27X	3	30	253.90	1.290
B	28X	1	60	260.60	1.237
B	28X	1	33	260.60	1.413
B	28X	2	33	262.10	1.051
B	28X	3	33	263.60	1.349
B	29X	1	50	270.20	1.362
B	29X	1	90	270.20	1.389
B	29X	2	10	271.70	1.416
B	30X	1	30	279.90	1.483
B	31X	1	60	289.60	1.252
B	31X	2	60	291.10	1.439
B	31X	3	60	292.60	1.536
B	31X	4	60	294.10	1.369
B	32X	1	80	299.30	1.407
B	32X	1	120	299.30	1.638
B	32X	2	80	300.80	1.739

Table 3 - 2

B	32X	3	80	302.30	1.321
B	33X	1	50	309.00	1.293
B	33X	2	50	310.50	1.417
B	33X	4	50	313.50	1.387
B	33X	5	50	315.00	1.241
B	34X	1	30	318.70	1.235
B	34X	2	46	320.20	1.581
B	35X	1	30	328.30	1.453
B	36X	1	80	337.90	1.478
B	36X	2	60	339.40	1.467
B	36X	3	50	340.90	1.628
B	37X	1	60	347.50	1.218
B	37X	2	40	348.70	1.455
B	38X	1	60	357.10	1.416
B	39X	1	60	366.70	1.936
B	40X	1	10	376.40	1.282
B	41X	1	15	386.00	1.230
C	2R	1	31	359.60	1.510
C	2R	1	31	359.60	1.530
C	3R	2	34	370.80	1.410
C	3R	2	34	370.80	1.380
C	4R	1	120	379.00	1.350
C	4R	1	120	379.00	1.370
C	5R	2	79	390.10	1.350
C	5R	2	91	390.10	1.430
C	5R	2	110	390.10	1.244
C	5R	2	91	390.10	1.360
C	5R	2	96	390.10	1.503
C	6R	1	91	398.30	1.590
C	6R	1	91	398.30	1.570
C	7R	1	18	408.00	1.390
C	7R	1	18	408.00	1.320
C	8R	3	8	420.70	1.250
C	8R	3	8	420.70	1.310
C	9R	3	88	430.30	1.340
C	9R	3	88	430.30	1.330
C	10R	4	38	441.00	1.300
C	10R	4	38	441.00	1.280
C	11R	3	102	449.00	2.100
C	11R	3	102	449.00	1.990
C	12R	5	69	461.20	1.720
C	12R	5	69	461.20	1.630
C	13R	2	131	466.10	1.600
C	13R	2	131	466.10	1.610
C	13R	3	0	467.60	1.290
C	13R	3	0	467.60	1.472
C	13R	3	0	467.60	1.440
C	14R	1	35	474.10	1.490
C	14R	1	35	474.10	1.420
C	16R	1	108	493.20	1.520
C	16R	1	108	493.20	1.600
C	17R	1	14	502.40	1.200
C	17R	1	14	502.40	1.240
C	18R	2	134	513.40	1.680
C	18R	2	134	513.40	1.640
C	23R	5	5	565.70	2.120
C	23R	5	5	565.70	2.000
C	24R	3	16	572.30	1.870
C	24R	3	16	572.30	1.840
C	25R	1	21	579.00	1.860

Table 3 - 3

C	25R	1	21	579.00	1.880
C	28R	1	73	607.00	1.070
C	28R	1	73	607.00	1.070
C	29R	2	45	617.97	1.149
C	29R	4	44	621.02	1.366
C	29R	6	43	624.17	1.275
C	30R	2	64	627.39	1.246
C	30R	2	64	627.39	1.172
C	30R	3	38	628.85	1.263
C	30R	3	38	628.85	1.409
C	30R	6	51	633.29	1.163
C	30R	6	51	633.29	1.394
C	31R	1	98	635.30	1.358
C	31R	1	31	635.30	1.094
C	31R	2	47	636.71	1.564
C	31R	3	101	638.18	1.257
C	31R	4	58	639.61	1.380
C	33R	2	30	656.18	1.206
C	33R	2	60	656.18	1.275
C	37R	3	101	696.00	1.400
C	37R	3	101	696.00	1.380
C	38R	5	5	708.50	1.380
C	38R	5	5	708.50	1.340
C	38R	5	5	708.50	1.360
C	39R	3	42	714.70	1.410
C	39R	3	42	714.70	1.380
C	40R	2	95	722.40	1.450
C	40R	2	95	722.40	1.490
C	42R	3	16	742.80	1.380
C	42R	3	16	742.80	1.370
<i>Basalts</i>					
D	1R	1	52	948.42	1.735
D	1R	1	52	948.42	1.725
D	1R	2	52	949.92	1.725
D	2R	2	0	956.09	1.105
D	2R	3	95	958.11	1.670
D	3R	1	33	964.73	1.695
D	4R	1	30	974.00	1.610
D	5R	1	133	984.53	1.675
D	5R	5	29	988.45	1.755
D	5R	7	129	992.29	1.760
D	6R	1	0	992.40	1.675
D	7R	1	81	1002.81	1.690
D	8R	1	28	1011.78	1.770
D	9R	1	72	1021.62	1.840
D	9R	1	72	1021.62	1.840
D	10R	1	64	1030.84	1.580
D	11R	1	90	1040.30	1.590
D	12R	1	26	1045.36	1.690
D	15R	1	55	1073.55	1.555
D	17R	2	103	1094.16	1.695
D	18R	1	10	1101.20	1.830
D	19R	1	114	1111.44	1.500
D	20R	2	71	1121.71	1.635
D	21R	1	113	1130.13	1.755
D	22R	1	15	1138.75	1.690
D	23R	2	20	1149.50	1.725
D	24R	4	42	1161.32	1.740
D	25R	1	125	1167.75	1.765
D	26R	2	92	1178.42	1.425

Table 3 - 4

D	27R	2	40	1186.95	1.725
---	-----	---	----	---------	-------

TABLE 4  
Thermal Conductivity Values for Site 766

SAMPLE ID				DEPTH mbsf	Thermal Conductivity W/m °C
<i>Sediments</i>					
A	1R	1	110	1.1	1.407
A	1R	2	40	1.9	1.095
A	1R	3	40	3.4	1.096
A	2R	1	50	8.2	1.228
A	2R	2	50	9.76	1.268
A	2R	3	55	11.31	1.137
A	2R	5	55	14.31	1.200
A	3R	2	45	19.25	1.270
A	3R	3	45	20.75	1.515
A	3R	4	45	22.25	1.593
A	3R	CC	10	26.40	1.529
A	4R	1	60	27.60	1.515
A	4R	2	60	29.10	1.374
A	5R	3	60	40.30	1.480
A	5R	6	30	44.50	1.412
A	6R	4	60	51.40	1.350
A	7R	1	40	56.40	1.089
A	7R	2	40	57.90	1.425
A	7R	4	33	60.83	1.413
A	7R	7	30	65.30	1.413
A	8R	1	50	66.20	1.412
A	8R	2	44	67.64	1.439
A	9R	1	60	75.90	1.417
A	9R	4	60	80.40	1.460
A	10R	1	70	85.70	1.340
A	10R	3	50	88.50	1.479
A	11R	3	40	98.10	1.630
A	11R	4	40	99.60	1.735
A	12R	1	40	104.70	1.659
A	12R	2	40	106.20	1.505
A	13R	1	40	114.30	1.742
A	13R	3	40	117.30	1.759
A	14R	1	40	124.00	1.512
A	14R	2	40	125.50	1.433
A	15R	2	101	135.71	0.977
A	15R	4	90	138.60	1.581
A	16R	2	120	145.60	1.367
A	16R	5	54	149.44	1.341
A	17R	2	70	154.70	1.436
A	17R	5	38	158.88	1.391
A	17R	7	20	161.70	1.294
A	18R	1	47	162.57	1.341
A	18R	3	34	165.44	1.276
A	18R	6	38	169.98	1.384
A	19R	1	78	172.48	1.396
A	19R	3	43	175.13	1.249
A	19R	5	32	178.02	1.216
A	20R	1	98	182.38	1.426
A	20R	2	40	183.30	1.439
A	20R	4	30	186.20	1.095
A	21R	1	43	191.43	1.472

A	21R	2	82	193.32	1.445
A	24R	1	110	221.00	1.669
A	25R	1	23	229.83	1.481
A	26R	2	70	241.50	1.226
A	26R	3	56	242.86	1.169
A	27R	1	114	250.04	0.864
A	27R	2	51	250.91	1.103
A	28R	2	53	260.63	1.242
A	28R	4	60	263.70	1.332
A	29R	1	80	269.10	1.142
A	29R	3	60	271.90	1.202
A	30R	2	80	280.20	1.048
A	30R	4	40	282.80	1.152
A	36R	1	52	336.32	1.346
A	36R	1	115	336.95	1.374
A	36R	2	16	337.46	1.399
A	37R	1	62	346.12	1.477
A	38R	1	75	355.85	1.574
A	38R	3	68	358.78	1.543
A	39R	1	78	365.58	1.351
A	39R	3	71	368.51	1.380
A	41R	1	116	385.36	1.345
A	42R	2	35	395.65	1.292
A	42R	4	35	398.65	1.325
A	42R	4	38	398.68	1.444
A	43R	2	35	405.35	1.300
A	43R	4	35	408.35	1.592
A	44R	2	50	415.20	1.465
A	44R	6	50	421.20	1.447
A	45R	3	50	426.30	1.522
A	45R	7	30	432.10	1.404
A	46R	3	50	436.04	1.422
A	46R	6	50	440.54	1.303
A	47R	2	50	444.20	1.339
A	47R	6	50	450.20	1.125
A	49R	4	77	466.77	1.490
<i>Basalts</i>					
A	50R	3	48	474.50	1.685
A	51R	3	86	484.21	1.680
A	52R	1	79	490.69	1.695
A	52R	3	0	492.97	1.820
A	53R	3	45	502.15	1.825
A	54R	4	67	512.93	1.800
A	55R	7	136	527.02	1.835

Table 4 - 2